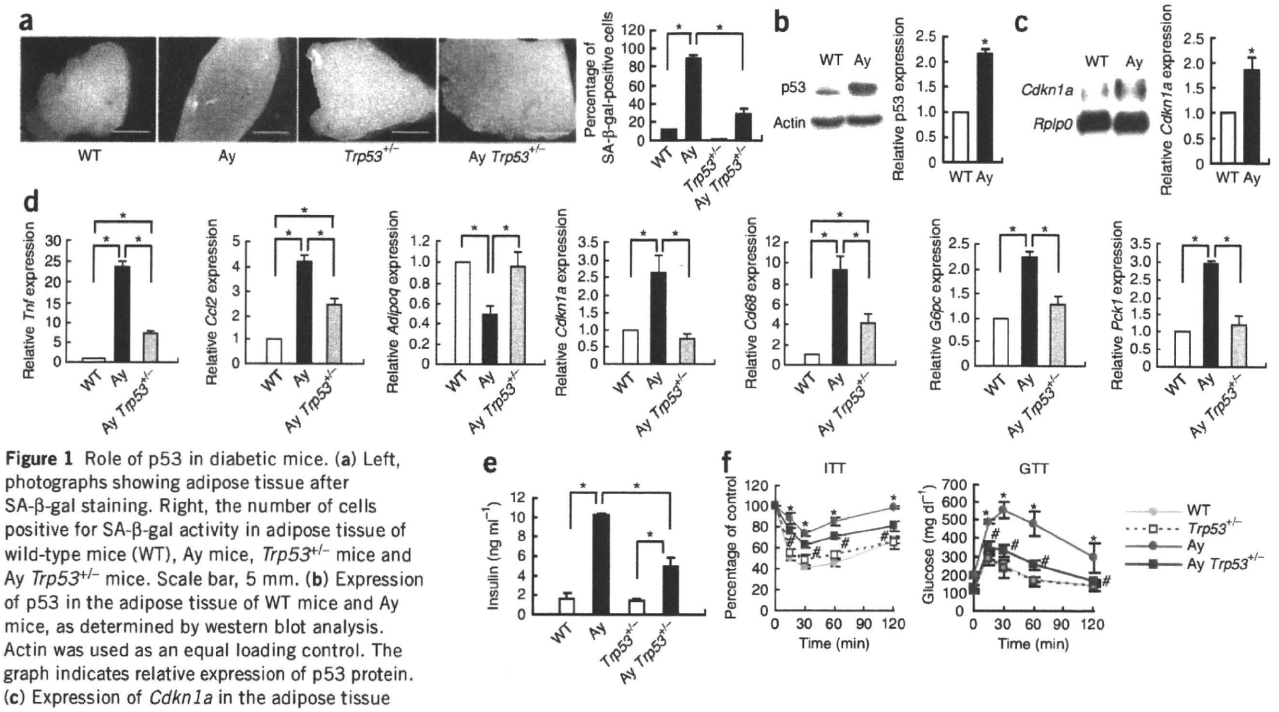

Figure 1 Role of p53 in diabetic mice. (**a**) Left, photographs showing adipose tissue after SA-β-gal staining. Right, the number of cells positive for SA-β-gal activity in adipose tissue of wild-type mice (WT), Ay mice, *Trp53*$^{+/-}$ mice and Ay *Trp53*$^{+/-}$ mice. Scale bar, 5 mm. (**b**) Expression of p53 in the adipose tissue of WT mice and Ay mice, as determined by western blot analysis. Actin was used as an equal loading control. The graph indicates relative expression of p53 protein. (**c**) Expression of *Cdkn1a* in the adipose tissue WT mice and Ay mice, as determined by northern blot analysis. Ribosomal protein, large, P0 (Rplp0) was used as an equal loading control. The graph indicates relative expression of *Cdkn1a* mRNA. (**d**) Real-time PCR assessing the expression of cytokines, *Cdkn1a* and *Cd68* in adipose tissue and the expression of *G6pc* (encoding glucose-6-phosphatase) and *Pck1* (encoding phosphoenolpyruvate carboxykinase) in the livers of WT mice, Ay mice and Ay *Trp53*$^{+/-}$ mice. (**e**) Plasma insulin concentrations in WT mice, Ay mice, *Trp53*$^{+/-}$ mice and Ay *Trp53*$^{+/-}$ mice. $^{*}P < 0.05$; $n = 4$–6 for **a** and **d**; $n = 3$ for **b**; $n = 4$ for **c** and **e**. (**f**) Insulin tolerance test (ITT) and glucose tolerance test (GTT) in WT mice, Ay mice, *Trp53*$^{+/-}$ mice and Ay *Trp53*$^{+/-}$ mice. $^{*}P < 0.05$ versus WT; $^{\#}P < 0.05$ versus Ay; $n = 7$. Data are shown as the means ± s.e.m.

of macrophage marker expression, whereas expression of anti-inflammatory cytokines (including adiponectin, (*Adipoq*)) was downregulated in the adipose tissue of Ay mice (**Fig. 1d**). We detected upregulation of inflammatory cytokines, as well as of p53 protein and *Cdkn1a* expression, in both the stromal vascular fraction (macrophage-rich fraction) and the adipose-rich fraction (**Supplementary Fig. 1b**), suggesting that senescence of both macrophages and adipocytes causes an inflammatory response that leads to insulin resistance.

We next investigated whether inhibition of p53 could reverse insulin resistance and glucose intolerance in Ay mice. The number of SA-β-gal–positive cells and the expression of *Cdkn1a* were significantly lower in adipose tissue from Ay *Trp53*$^{+/-}$ mice than in tissue from Ay *Trp53*$^{+/+}$ mice (**Fig. 1a,d**), whereas there was no significant difference in food intake between the two groups (**Supplementary Fig. 1c**). The fat weight of Ay *Trp53*$^{+/-}$ mice was slightly lower than that of Ay *Trp53*$^{+/+}$ mice (**Supplementary Fig. 2a**). Reduced activation of p53 led to lower plasma insulin concentrations in Ay mice and also to normalization of cytokine and macrophage marker expression by adipose tissue (**Fig. 1d,e**). Hepatic expression of gluconeogenic enzymes was also lower in Ay *Trp53*$^{+/-}$ mice (**Fig. 1d**). Consistent with these changes, Ay *Trp53*$^{+/-}$ mice showed significantly better insulin sensitivity and glucose tolerance compared with Ay *Trp53*$^{+/+}$ mice as determined by insulin and glucose tolerance tests (**Fig. 1f**).

Because Ay *Trp53*$^{+/-}$ mice have p53 haploinsufficiency throughout the whole body, improvement of insulin resistance might be attributable to inhibition of p53 activity in other tissues aside from the white adipose tissue. To investigate the role of adipose tissue p53 in the regulation of insulin resistance, we generated mice with adipocyte-specific p53 deficiency (adipo-p53–deficient mice), using transgenic mice that express Cre recombinase under control of the mouse fatty acid–binding protein-4 (*Fabp4*) promoter, and fed these mice a high-fat, high-sucrose (HF-HS) diet for 4 months. Expression of p53 protein and *Cdkn1a* mRNA in adipose tissue was significantly upregulated in littermate control mice on the HF-HS diet, whereas this increase was significantly attenuated in adipo-p53–deficient mice (*Trp53*$^{loxP/loxP}$ Fabp4-Cre) receiving the same diet (**Fig. 2a,b** and **Supplementary Fig. 1d**). These mice had a slightly smaller increase of fat weight (**Supplementary Fig. 2b**) and normalized expression of adipokines and hepatic gluconeogenic enzymes (**Fig. 2b**), whereas hepatic p53 protein expression was unchanged (**Fig. 2a**). Insulin-induced phosphorylation of Akt was also restored in adipo-p53–deficient mice (**Supplementary Fig. 1e**). Consequently, insulin resistance induced by the HF-HS diet was lower in mice with adipocyte-specific ablation of p53 compared to control mice (**Fig. 2c**), indicating that p53 expression in adipose tissue has a crucial role in the development of insulin resistance.

It has been reported that Fabp4 is expressed in hematopoietic cells and has considerable influence on various biological responses[14,15]. To examine the possible involvement of p53 in hematopoietic cells, we transplanted wild-type bone marrow cells into adipo-p53–deficient mice or littermate control mice and induced dietary obesity in these mice. Adipo-p53–deficient mice transplanted with wild-type bone marrow cells showed better glucose tolerance than littermate control mice transplanted with wild-type marrow cells, but their glucose tolerance was impaired compared with that of adipo-p53–deficient mice without bone marrow transplantation (**Supplementary Fig. 1f**). In adipose-p53–deficient mice, expression of p53 protein and *Cdkn1a* was considerably lower in both the stromal vascular fraction and the

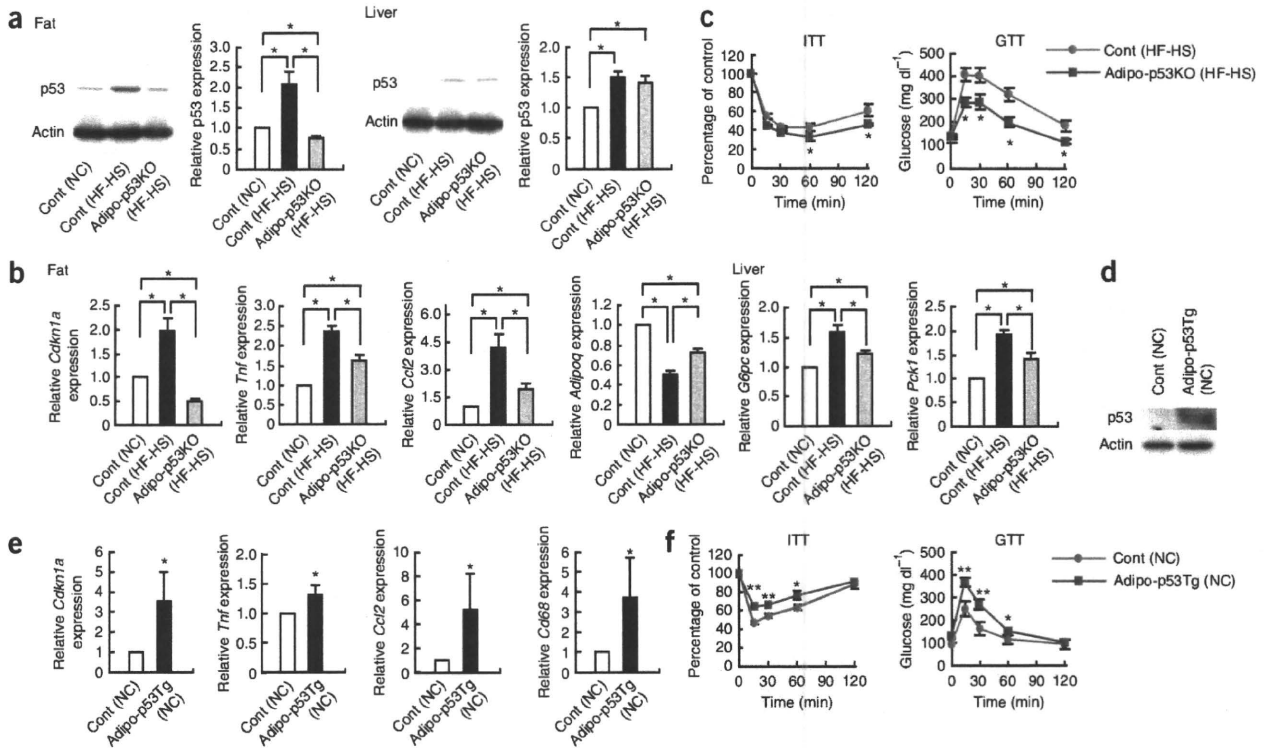

Figure 2 Adipose tissue p53 expression contributes to insulin resistance in mice with dietary obesity. (**a**) Western blot analysis for p53 in the fat and liver of littermate controls (Cont) on a normal diet (normal chow, NC), littermate controls (Cont) on an HF-HS diet (HF-HS), and adipo-p53–deficient mice (Adipo-p53KO) on an HF-HS diet (HF-HS). The graph indicates relative expression of p53 protein. (**b**) Real-time PCR assessing the expression of *Cdkn1a*, *Tnf*, *Ccl2* and *Adipoq* in adipose tissue and *G6pc* and *Pck1* in liver of the same mice as in **a**. $*P < 0.05$; $n = 5$ mice for **a** and **b**. (**c**) ITT and GTT in Adipo-p53KO mice and littermate controls (Cont) after 4 months on a HF-HS diet or a normal diet. $*P < 0.05$ versus control (HF-HS); $n = 8$. (**d**) Western blot analysis for p53 in adipose tissue of littermate controls (Cont) and adipo-p53–transgenic (Adipo-p53Tg) mice on a normal diet (NC). (**e**) Real-time PCR assessing the expression of *Cdkn1a*, *Tnf*, *Ccl2* and *Cd68* in adipose tissue of the same mice as in **d**. $*P < 0.05$; $n = 5$. (**f**) ITT and GTT in Adipo-p53Tg mice and littermate controls (Cont) on a normal diet (NC). $*P < 0.05$, $**P < 0.01$ versus control; $n = 8$. Data are shown as the means ± s.e.m.

adipose-rich fraction compared with the levels seen in littermate control mice (**Supplementary Fig. 1d**). These results suggested that both macrophages and adipocytes contribute to the senescence-like changes of adipose tissues in mice with dietary obesity and that upregulation of p53 expression in adipose tissue has a pathological role in producing insulin resistance.

To further investigate the role of adipose tissue p53, we established transgenic mice that showed an increase of p53 protein and *Cdkn1a* mRNA expression in adipose tissue (**Fig. 2d,e**). Consistent with the results found in adipose-p53–deficient mice, these transgenic mice on a normal diet showed higher expression of proinflammatory cytokines and a macrophage marker (**Fig. 2e**), which was associated with impairment of insulin sensitivity and glucose tolerance (**Fig. 2f**), providing further evidence for a major role for adipose tissue p53 in insulin resistance.

Insulin resistance has been reported to correlate with enhanced telomere shortening in young adults[16], whereas aging is known to accelerate telomere dysfunction in various human tissues[1,5]. It is well accepted that dysfunctional (that is, critically short) telomeres resemble damaged DNA and thus trigger a p53-dependent response[17,18]. To investigate a potential relationship between telomere-dependent p53 activation and insulin resistance, we used telomerase reverse transcriptase (*Tert*)-deficient mice. These mice have a normal phenotype in the first generation (G1), presumably because mice possess very long telomeres[19,20]. However, their telomeres become shorter with successive generations, and the mice eventually become infertile by the fourth to sixth generation (G4–G6), owing to impairment of the reproductive system[20]. We fed an HF-HS diet to G4 mice for 8 weeks (from 4 to 12 weeks of age) and examined the effects of cellular aging on glucose metabolism. Although the insulin sensitivity and glucose tolerance of G4 mice were similar to those of wild-type mice on a normal diet, insulin resistance and glucose intolerance became more prominent in G4 mice than in wild-type mice after feeding with the HF-HS diet (**Fig. 3a**). There were no significant differences in weight gain, food intake and oxygen consumption between the two groups (**Fig. 3b**). Expression of proinflammatory cytokines such as *Tnf* and *Ccl2* was increased in the adipose tissue of G4 mice on the HF-HS diet, and this increase was evident in mice with shorter telomeres in adipose cells (**Fig. 3c,d** and **Supplementary Fig. 3a**). Shorter telomeres also promoted the infiltration of macrophages into adipose tissue (**Fig. 3c** and **Supplementary Figs. 2c** and **3b**). Expression of hepatic gluconeogenic enzymes was upregulated in G4 mice (**Fig. 3c**). Insulin-induced phosphorylation of Akt was markedly lower in the liver of G4 mice compared to wild-type mice, and in skeletal muscle to a lesser extent (**Supplementary Fig. 3c**). The adipose tissue of G4 mice on the HF-HS diet showed senescence-like changes, including

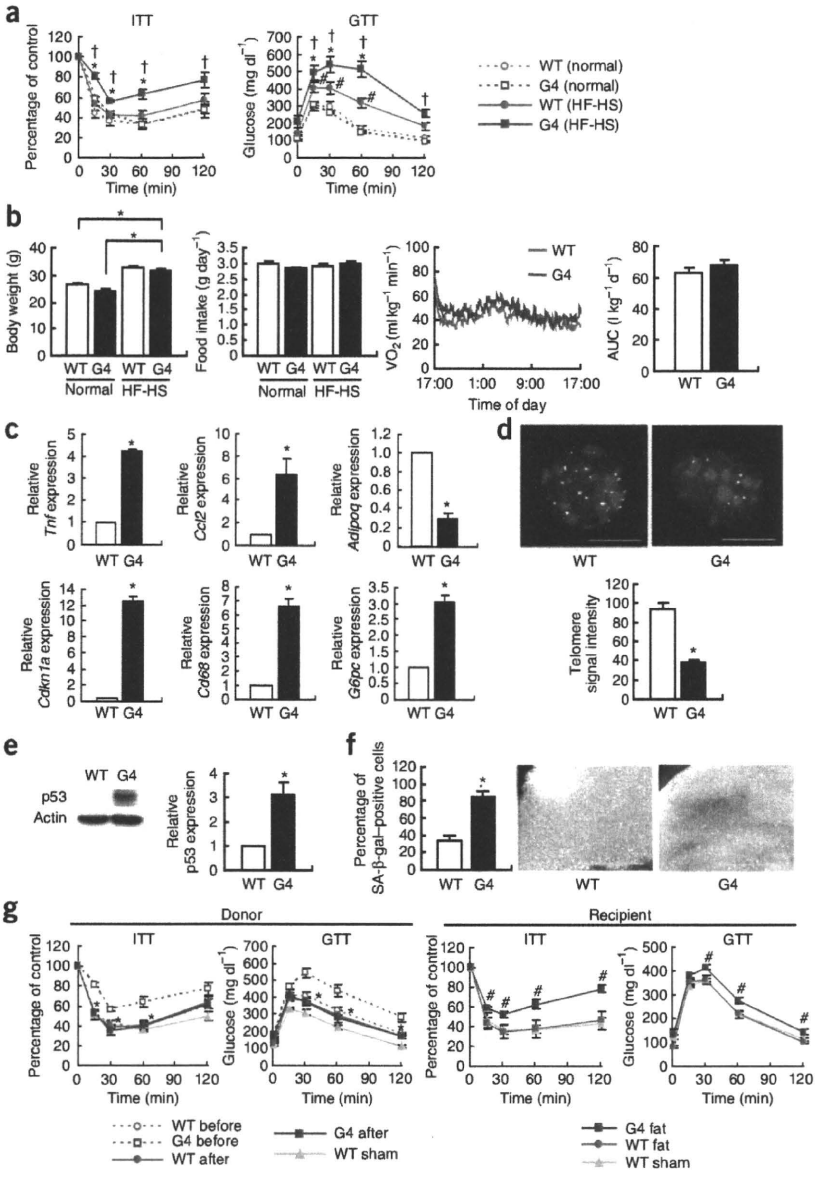

Figure 3 Adipose tissue p53 expression and insulin resistance in G4 mice. (**a**) ITT and GTT after 8 weeks on a HF-HS diet or a normal diet (normal) in G4 and WT mice. $*P < 0.05$ versus WT (HF-HS); $\#P < 0.05$ versus WT (normal); $\dagger P < 0.05$ versus G4 (normal); $n = 7$. (**b**) Body weight, food intake and oxygen consumption (VO_2) in WT and G4 mice. AUC, area under the curve. (**c**) Real-time PCR analysis of the expression of cytokines, *Cdkn1a* and *Cd68* in adipose tissue and the expression of *G6pc* in the livers of WT mice and G4 mice. All mice were fed on the HF-HS diet. (**d**) Top, telomeric fluorescence (yellow) *in situ* hybridization of adipocytes from WT and G4 mice. The signal intensity of the X chromosome (red) was used as an internal control. Bottom, estimation of the length of telomeres in adipose cells by quantification of telomeric fluorescence *in situ* hybridization images. Representative of 30 nuclei (images) for each genotype. Scale bar, 10 μm. (**e**) Expression of p53 in the adipose tissue of WT mice and G4 mice on the HF-HS diet, as determined by western blot analysis. The graph indicates relative expression of p53 protein. (**f**) The number of cells positive for SA-β-gal activity in the adipose tissue of WT mice and G4 mice. Photographs show adipose tissue after SA-β-gal staining. Scale bar, 5 mm. $*P < 0.05$; $n = 6$ for **b**; $n = 5$ for **c**; $n = 30$ nuclei for **d**; $n = 3$ for **e** and **f**. (**g**) Left, ITT and GTT in WT and G4 donor mice before and after fat pad removal. Right, ITT and GTT in recipients of fat pads (1 g) from WT mice (WT fat) or G4 mice (G4 fat) and in sham-operated WT mice (WT sham). $*P < 0.05$ versus G4 before, $\#P < 0.05$ versus WT fat; $n = 6$. Data are shown as the means ± s.e.m.

increased expression of *Cdkn1a* mRNA and p53 protein, as well as enhanced activity of SA-β-gal (**Fig. 3c,e,f** and **Supplementary Fig. 3d**). These results suggest that telomere-dependent senescence of adipose tissue can also promote an inflammatory response, thereby leading to insulin resistance.

To investigate the influence of adipose tissue senescence on the insulin resistance of G4 mice receiving a HF-HS diet, we transplanted epididymal fat pads subcutaneously into wild-type mice and examined the changes of insulin sensitivity and glucose tolerance in the donor and recipient mice. Two weeks after fat pad removal, insulin resistance and glucose intolerance were both markedly improved in G4 mice on the HF-HS diet (**Fig. 3g** and **Supplementary Fig. 2d**). The insulin level of donor G4 mice was also normalized by 2 weeks after fat pad removal (**Supplementary Fig. 3e**). Conversely, implantation of adipose tissue from G4 mice on this diet significantly impaired the insulin sensitivity and glucose tolerance of wild-type recipient mice, whereas implantation of adipose tissue from other wild-type mice fed the same diet had no effect (**Fig. 3g**). Implantation of adipose tissue from G4 mice also lowered insulin-induced phosphorylation of Akt in the liver (**Supplementary Fig. 3f**). Histological examination showed that the implanted adipose tissue was viable and vascularized (**Supplementary Fig. 3g**). Moreover, implantation of fat pads collected from G4 $Trp53^{+/-}$ mice into wild-type mice had less influence on the insulin resistance and glucose tolerance of the recipients (**Supplementary Fig. 3h**) compared with fat pads from G4 $Trp53^{+/+}$ mice. These results indicate that telomere-dependent p53 activation in adipose tissue also leads to insulin resistance.

We noted that expression of histone γ-H2AX, a marker of double-stranded DNA breaks, was increased in the adipose tissue of Ay mice as well as G4 mice (**Fig. 4a**), suggesting a potential role of the ROS-induced DNA damage pathway in the development of type 2 diabetes. To further investigate the relationship between ROS-induced DNA damage and diabetes, we examined the effect of oxidative stress on the expression of inflammatory cytokines in primary cultures of human preadipocytes. Treatment with hydrogen peroxide led to a marked increase of p53 protein expression (**Fig. 4b**). Hydrogen peroxide treatment significantly upregulated expression of *TNF* and *CCL2*, whereas this upregulation was inhibited by p53 knockdown (**Fig. 4c**). This treatment also increased the activity of nuclear factor-κB (NF-κB;

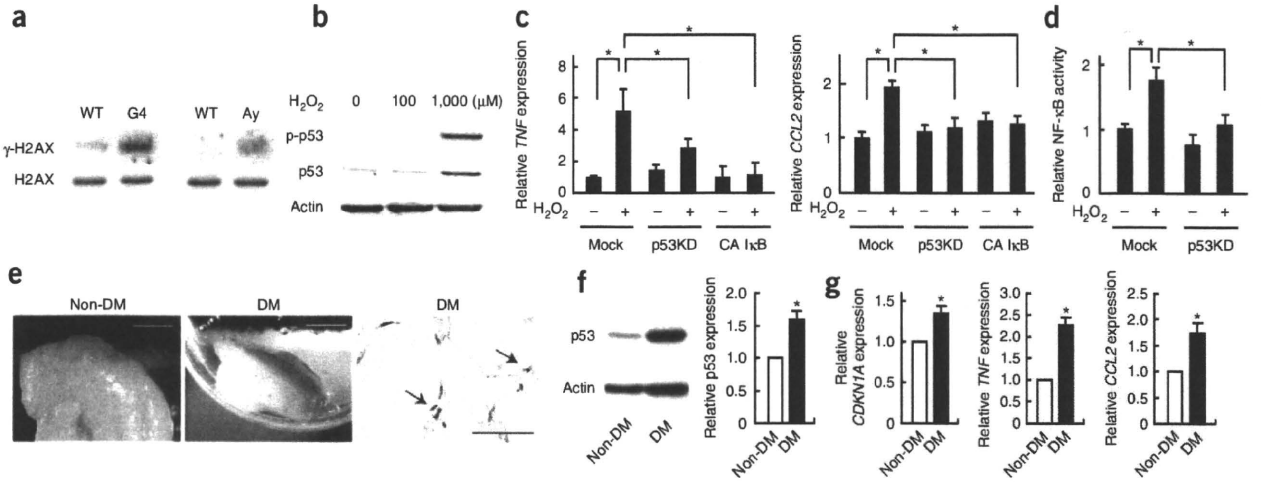

Figure 4 Senescence-like features of adipose tissue from subjects with diabetes. (**a**) Western blot analysis of γ-H2AX expression in adipose tissue of WT mice and G4 mice on a HF-HS diet and WT mice and Ay mice on a normal diet. (**b**) Effect of hydrogen peroxide (H_2O_2) on p53 expression in human preadipocytes by western blot analysis. p-p53, phosphorylated p53. (**c**) Hydrogen peroxide–induced expression of *TNF* and *CCL2* in human preadipocytes transfected with siRNA targeting p53 (p53KD) or the vector encoding constitutively active inhibitor of κB (CA IκB). (**d**) Effect of p53 knockdown (p53KD) on hydrogen peroxide–induced activation of NF-κB. (**e**) Adipose tissue from subjects without diabetes (non-DM) or subjects with diabetes (DM) after SA-β-gal staining. Scale bar, 10 mm. The photograph on the right shows adipose tissue obtained from a subject with diabetes (DM). Arrows indicate SA-β-gal–positive cells. Scale bar, 50 μm. (**f**,**g**) Expression of p53, *CDKN1A* and cytokines in adipose tissue obtained from subjects without diabetes or subjects with diabetes, as determined by western blot analysis (**f**) or real-time PCR (**g**). The graphs indicate relative expression of p53 protein (**f**) and relative mRNA levels of *CDKNA1*, *TNF* and *CCL2* (**g**). $^*P < 0.05$; $n = 5$ for **c**, **d**, **f** and **g**. Data are shown as the means ± s.e.m.

Fig. 4d), a key transcription factor that regulates the induction of cytokines, including *TNF* and *CCL2*, whereas inhibition of NF-κB activation suppressed oxidative stress–induced upregulation of these cytokines (**Fig. 4c**). In agreement with previous reports that induction of p53 causes activation of NF-κB[21,22], we found that p53 deficiency led to a decrease in oxidative stress–induced NF-κB activation (**Fig. 4d**), indicating that ROS-induced p53 activation causes NF-κB–dependent induction of inflammatory cytokines and thus accelerates the development of diabetes.

To determine whether or not senescence-like changes occur in human adipose tissue, we examined visceral fat obtained from subjects undergoing abdominal surgery for primary gastric cancer or colon cancer. Adipose tissue from subjects with diabetes showed increased SA-β-gal activity and higher levels of p53 protein and *CDKN1A* mRNA expression compared with tissue from nondiabetic subjects (**Fig. 4e–g**). Moreover, expression of inflammatory cytokines was significantly increased in diabetic adipose tissue (**Fig. 4g**), suggesting that aging of fat cells has a major role in human diabetes.

Recent studies have shown that longevity signals generated in adipose tissue are crucial in regulating the lifespan of various species, ranging from worms to mice, and suggested that aging is non–cell-autonomously regulated by adipose tissue[23–26]. Consistent with these reports, subcutaneous implantation of senescent adipose tissue from G4 mice accelerates the senescence of epididymal fat in wild-type recipients (T.M., unpublished data). Senescence of adipose tissue may increase the local production of proinflammatory molecules, and it also promotes systemic inflammation and insulin resistance via non–cell-autonomous mechanisms. In contrast, low circulating insulin concentrations are generally associated with longevity, and the activation of longevity signals in adipose tissue has been reported to lower the circulating insulin level and extend the lifespan[27,28]. We found that inhibition of p53 activity in adipose tissue improved insulin resistance and decreased the plasma insulin level. Thus, p53 activation in adipose tissue may be a proaging signal with a negative influence on longevity, whereas inhibition of cellular aging may become a new strategy for the treatment of diabetes as well as aging and its associated diseases.

METHODS

Methods and any associated references are available in the online version of the paper at http://www.nature.com/naturemedicine/.

Note: Supplementary information is available on the Nature Medicine website.

ACKNOWLEDGMENTS

We thank H. Karagiri for discussion, W.C. Greene (University of California) and T. Fujita (The Tokyo Metropolitan Institute of Medical Science) for expression vector encoding constitutively active IκB and p55-A2-Luc (luciferase reporter vector containing the κB binding sites), respectively, A. Berns (The Netherlands Cancer Institute) for floxed *Trp53* mice, and E. Fujita, Y. Ishiyama, R. Kobayashi and Y. Ishikawa for their excellent technical assistance. This work was supported by a Grant-in-Aid for Scientific Research from the Ministry of Education, Science, Sports and Culture and Health and Labor Sciences Research Grants (to I.K.); a Grant-in-Aid for Scientific Research from the Ministry of Education, Culture, Sports, Science and Technology of Japan; and grants from the Suzuken Memorial Foundation, the Japan Diabetes Foundation, the Ichiro Kanehara Foundation, the Tokyo Biochemical Research Foundation, the Takeda Science Foundation, the Cell Science Research Foundation and the Japan Foundation of Applied Enzymology (to T.M.).

AUTHOR CONTRIBUTIONS

T.M. designed and conducted experiments and wrote the manuscript, M.O., I.S., T.K., M.Y., T.I., A. Nojima and Y.O. conducted experiments, A. Nabetani performed telomere analysis, H.M. performed the human studies, F.I. generated telomerase-deficient mice and I.K. evaluated the results, supervised this study and wrote the manuscript.

Published online at http://www.nature.com/naturemedicine/.
Reprints and permissions information is available online at http://npg.nature.com/reprintsandpermissions/.

1. Stewart, S.A. & Weinberg, R.A. Telomeres: cancer to human aging. *Annu. Rev. Cell Dev. Biol.* **22**, 531–557 (2006).
2. Serrano, M. & Blasco, M.A. Putting the stress on senescence. *Curr. Opin. Cell Biol.* **13**, 748–753 (2001).
3. Campisi, J. Senescent cells, tumor suppression, and organismal aging: good citizens, bad neighbors. *Cell* **120**, 513–522 (2005).

4. Shay, J.W. & Wright, W.E. Senescence and immortalization: role of telomeres and telomerase. *Carcinogenesis* **26**, 867–874 (2005).
5. Minamino, T. & Komuro, I. Vascular cell senescence: contribution to atherosclerosis. *Circ. Res.* **100**, 15–26 (2007).
6. Minamino, T. & Komuro, I. Vascular aging: insights from studies on cellular senescence, stem cell aging, and progeroid syndromes. *Nat. Clin. Pract. Cardiovasc. Med.* **5**, 637–648 (2008).
7. Greider, C.W. Telomere length regulation. *Annu. Rev. Biochem.* **65**, 337–365 (1996).
8. Herbig, U., Ferreira, M., Condel, L., Carey, D. & Sedivy, J.M. Cellular senescence in aging primates. *Science* **311**, 1257 (2006).
9. Dimri, G.P. *et al.* A biomarker that identifies senescent human cells in culture and in aging skin in vivo. *Proc. Natl. Acad. Sci. USA* **92**, 9363–9367 (1995).
10. Furukawa, S. *et al.* Increased oxidative stress in obesity and its impact on metabolic syndrome. *J. Clin. Invest.* **114**, 1752–1761 (2004).
11. Hotamisligil, G.S., Shargill, N.S. & Spiegelman, B.M. Adipose expression of tumor necrosis factor-α: direct role in obesity-linked insulin resistance. *Science* **259**, 87–91 (1993).
12. Weisberg, S.P. *et al.* Obesity is associated with macrophage accumulation in adipose tissue. *J. Clin. Invest.* **112**, 1796–1808 (2003).
13. Kamei, N. *et al.* Overexpression of monocyte chemoattractant protein-1 in adipose tissues causes macrophage recruitment and insulin resistance. *J. Biol. Chem.* **281**, 26602–26614 (2006).
14. Makowski, L. *et al.* Lack of macrophage fatty-acid–binding protein aP2 protects mice deficient in apolipoprotein E against atherosclerosis. *Nat. Med.* **7**, 699–705 (2001).
15. Makowski, L., Brittingham, K.C., Reynolds, J.M., Suttles, J. & Hotamisligil, G.S. The fatty acid–binding protein, aP2, coordinates macrophage cholesterol trafficking and inflammatory activity. Macrophage expression of aP2 impacts peroxisome proliferator–activated receptor γ and IκB kinase activities. *J. Biol. Chem.* **280**, 12888–12895 (2005).
16. Gardner, J.P. *et al.* Rise in insulin resistance is associated with escalated telomere attrition. *Circulation* **111**, 2171–2177 (2005).
17. Chin, L. *et al.* p53 deficiency rescues the adverse effects of telomere loss and cooperates with telomere dysfunction to accelerate carcinogenesis. *Cell* **97**, 527–538 (1999).
18. Karlseder, J., Broccoli, D., Dai, Y., Hardy, S. & de Lange, T. p53- and ATM-dependent apoptosis induced by telomeres lacking TRF2. *Science* **283**, 1321–1325 (1999).
19. Blasco, M.A. *et al.* Telomere shortening and tumor formation by mouse cells lacking telomerase RNA. *Cell* **91**, 25–34 (1997).
20. Lee, H.W. *et al.* Essential role of mouse telomerase in highly proliferative organs. *Nature* **392**, 569–574 (1998).
21. Ryan, K.M., Ernst, M.K., Rice, N.R. & Vousden, K.H. Role of NF-κB in p53-mediated programmed cell death. *Nature* **404**, 892–897 (2000).
22. Benoit, V. *et al.* Transcriptional activation of cyclooxygenase-2 by tumor suppressor p53 requires nuclear factor-κB. *Oncogene* **25**, 5708–5718 (2006).
23. Kenyon, C. The plasticity of aging: insights from long-lived mutants. *Cell* **120**, 449–460 (2005).
24. Hwangbo, D.S., Gershman, B., Tu, M.P., Palmer, M. & Tatar, M. *Drosophila* dFOXO controls lifespan and regulates insulin signalling in brain and fat body. *Nature* **429**, 562–566 (2004).
25. Giannakou, M.E. *et al.* Long-lived *Drosophila* with overexpressed dFOXO in adult fat body. *Science* **305**, 361 (2004).
26. Blüher, M., Kahn, B.B. & Kahn, C.R. Extended longevity in mice lacking the insulin receptor in adipose tissue. *Science* **299**, 572–574 (2003).
27. Blüher, M. *et al.* Adipose tissue selective insulin receptor knockout protects against obesity and obesity-related glucose intolerance. *Dev. Cell* **3**, 25–38 (2002).
28. Libina, N., Berman, J.R. & Kenyon, C. Tissue-specific activities of *C. elegans* DAF-16 in the regulation of lifespan. *Cell* **115**, 489–502 (2003).

ONLINE METHODS

Animal models. The study protocol was approved by the Chiba University Institutional Animal Care and Use Committee. The creation of mice deficient in *Tert* has been described previously[29]. We backcrossed heterozygous mice with wild-type C57BL/6 mice (SLC) for six generations and intercrossed them to produce G1 $Tert^{-/-}$ mice. Mating of G1 $Tert^{-/-}$ mice with each other generated G2 mice, after which we produced $Tert^{-/-}$ mice up to the fourth generation (G4). We purchased p53-deficient mice (with a C57BL/6 background) from Jackson Laboratories and mated them with $Tert^{+/-}$ mice to generate double heterozygotes ($Tert^{+/-}$ $Trp53^{+/-}$). We intercrossed these mice to generate G1 $Tert^{-/-}$ $Trp53^{+/-}$ mice. We mated G1 $Tert^{-/-}$ $Trp53^{+/-}$ mice with other G1 mice to produce G2 $Tert^{-/-}$ $Trp53^{+/-}$ mice, after which we repeated this mating strategy to generate G4 $Tert^{-/-}$ $Trp53^{+/-}$ mice. We fed the mice a HF-HS diet (Oriental Yeast)[30] or normal chow from 4 to 12 weeks of age before we performed metabolic analyses. We purchased Ay mice (with a C57BL/6 background) from Jackson Laboratories and mated them with $Trp53^{+/-}$ mice to generate $Trp53^{+/+}$, Ay $Trp53^{+/+}$, $Trp53^{+/-}$ and Ay $Trp53^{+/-}$ mice. We fed these mice normal chow and analyzed them at 20 weeks of age. We purchased mice that express Cre recombinase in adipocytes (Fabp4-Cre) from Jackson Laboratories. We then crossed Fabp4-Cre mice (with a C57BL/6 background) with mice that carry floxed *Trp53* alleles (with a C57BL/6 background)[31] to generate adipocyte-specific p53-knockout mice. We fed these mice a HF-HS diet or normal chow for 4 months before we performed metabolic analyses. Littermate controls had the genotype $Cre^{-}Trp53^{loxP/-}$ or $Cre^{-}Trp53^{loxP/loxP}$. We also generated transgenic mice (with a C57BL/6 background) that carry the *loxP-LacZ-loxP* cassette flanked by the *TP53* complementary DNA fragment under the control of the cytomegalovirus enhancer–chicken actin promoter. Expression of transgene-derived *TP53* was prevented by the *loxP-LacZ-loxP* cassette. When we bred these transgenic mice with Fabp4-Cre mice, the floxed *LacZ* cassette was excised in the resulting offspring ($Cre^{+}LacZ$-$TP53^{+}$), and we observed upregulation of p53 expression in adipose tissue (adipo-p53–transgenic mice). We fed these mice normal chow and analyzed them at 10–12 weeks of age. Littermate controls had the genotype $Cre^{-}LacZ$-$TP53^{+}$.

Cell culture. We purchased human preadipocytes from Sanko, and we cultured them according to the manufacturer's instructions.

Western blot analysis. We resolved whole-cell lysates (30–50 μg) by SDS PAGE. We transferred the proteins onto a polyvinylidene difluoride (PVDF) membrane (Millipore) incubated them with the primary antibody (**Supplementary Methods**), followed by incubation with rabbit IgG–specific horseradish peroxidase–conjugated antibody (111-035-003) or mouse IgG–specific horseradish peroxidase–conjugated antibody (115-035-003; Jackson). We detected specific proteins by enhanced chemiluminescence (Amersham).

Human subjects. The ethical committee of Chiba University Graduate School of Medicine reviewed and approved the study protocol. We enrolled 10 subjects (56–68 years old; six males and four females) who were admitted to Chiba University Hospital and underwent surgery for primary gastric or colon cancer. We obtained informed consent from all subjects before inclusion in the study.

Statistical analyses. Data are shown as the means ± s.e.m. We examined differences between groups by Student's *t* test or analysis of variance followed by Bonferroni's correction for comparison of means. For all analyses, we considered $P < 0.05$ as statistically significant.

Additional methods. Detailed methodology is described in the **Supplementary Methods**.

29. Yuan, X. *et al.* Presence of telomeric G-strand tails in the telomerase catalytic subunit TERT knockout mice. *Genes Cells* **4**, 563–572 (1999).
30. Maeda, N. *et al.* Diet-induced insulin resistance in mice lacking adiponectin/ACRP30. *Nat. Med.* **8**, 731–737 (2002).
31. Marino, S., Vooijs, M., van Der Gulden, H., Jonkers, J. & Berns, A. Induction of medulloblastomas in p53-null mutant mice by somatic inactivation of Rb in the external granular layer cells of the cerebellum. *Genes Dev.* **14**, 994–1004 (2000).

Hypertension Research (2009), 1–9

www.nature.com/hr

ORIGINAL ARTICLE

Multivalent ligand–receptor interactions elicit inverse agonist activity of AT_1 receptor blockers against stretch-induced AT_1 receptor activation

Yingjie Qin[1,3,4], Noritaka Yasuda[1,3], Hiroshi Akazawa[1], Kaoru Ito[1], Yoko Kudo[1], Chien-hui Liao[1], Rie Yamamoto[1], Shin-ichiro Miura[2], Keijiro Saku[2] and Issei Komuro[1]

Type 1 angiotensin II (AT_1) receptor has a critical role in the development of load-induced cardiac hypertrophy. Recently, we showed that mechanical stretching of cells activates the AT_1 receptor without the involvement of angiotensin II (AngII) and that this AngII-independent activation is inhibited by the inverse agonistic activity of the AT_1 receptor blocker (ARB), candesartan. Although the inverse agonist activity of ARBs has been studied in terms of their action on constitutively active AT_1 receptors, the structure–function relationship of the inverse agonism they exert against stretch-induced AT_1 receptor activation has not been fully elucidated. Assays evaluating *c-fos* gene expression and phosphorylated extracellular signal-regulated protein kinases (ERKs) have shown that olmesartan has strong inverse agonist activities against the constitutively active AT_1 receptor and the stretch-induced activation of AT_1 receptor, respectively. Ternary drug–receptor interactions, which occur between the hydroxyl group of olmesartan and Tyr^{113} and between the carboxyl group of olmesartan and Lys^{199} and His^{256}, were essential for the potent inverse agonist action olmesartan exerts against stretch-induced ERK activation and the constitutive activity of the AT_1-N111G mutant receptor. Furthermore, the inverse agonist activity olmesartan exerts against stretch-induced ERK activation requires an additional drug–receptor interaction involving the tetrazole group of olmesartan and Gln^{257} of the AT_1 receptor. These results suggest that multivalent interactions between an inverse agonist and the AT_1 receptor are required to stabilize the receptor in an inactive conformation in response to the distinct processes that lead to an AngII-independent activation of the AT_1 receptor.

Hypertension Research advance online publication, 7 August 2009; doi:10.1038/hr.2009.117

Keywords: angiotensin II; cardiac hypertrophy; G protein-coupled receptor; inverse agonist; mechanical stress

INTRODUCTION

The type 1 angiotensin II (AT_1) receptor is a member of the G protein-coupled receptor (GPCR) family and mediates most of the actions that angiotensin II (AngII) exerts on the cardiovascular system.[1] AT_1 receptor blockers (ARBs) are non-peptide compounds that selectively bind to the AT_1 receptor and inhibit AngII-induced receptor activation. At present, several ARBs are clinically available as a highly effective and well-tolerated class of drugs for the management of hypertension. In addition, clinical trials have indicated that ARBs provide cardiovascular protection that extends beyond blood pressure lowering.[2] Treatment with ARBs effectively prevents cardiac hypertrophy and improves cardiovascular outcomes in patients with hypertension.[2,3] Structurally, most ARBs have a common biphenyl-tetrazole ring and unique side chains, which contribute to drug-specific differences in their pharmacokinetic and pharmacodynamic properties.[2,4] These structural and pharmacological differences among ARBs may have an impact on long-term cardiovascular outcomes, although the clinical significance of these differences remains to be determined in large-scale trials.

Recent studies have shown that most GPCRs, including the AT_1 receptor, show spontaneous activity even in the absence of an agonist.[5] The AT_1 receptor is also activated by the mechanical stress of cellular stretching without the involvement of AngII.[6,7] A ligand capable of suppressing the agonist-independent activities of a receptor is defined as an inverse agonist.[5,8] We have previously reported that pressure overload induces cardiac hypertrophy in angiotensinogen-deficient mice as well as in wild-type (WT) mice and that hypertrophy is significantly attenuated by the inverse agonist, candesartan.[6] Therefore, the inverse agonist activities of ARBs have potential therapeutic benefits, at least in the prevention of load-induced cardiac hypertro-

[1]Department of Cardiovascular Science and Medicine, Chiba University Graduate School of Medicine, Chuo-ku, Chiba, Japan and [2]Department of Cardiology, Fukuoka University School of Medicine, Jonan-ku, Fukuoka, Japan
[3]These authors contributed equally to this work.
[4]Current address: Department of Cardiology, Affiliated Hospital of Chengde Medical College, No.36 Nanyingzi Street, Chengde, Hebei 067000, China
Correspondence: Dr I Komuro, Department of Cardiovascular Science and Medicine, Chiba University Graduate School of Medicine, 1-8-1 Inohana, Chuo-ku, Chiba 260-8670, Japan.
E-mail: komuro-tky@umin.ac.jp
Received 13 April 2009; revised 16 June 2009; accepted 18 June 2009

phy. The structural features that are required for the inverse agonist properties of some ARBs have been studied in constitutively active AT_1 receptors that have an Asn^{111} mutation. For example, the ternary interactions between the hydroxyl group of the imidazole ring and Tyr^{113} of the AT_1 receptor and between the carboxyl group and Lys^{199} and His^{256} of the AT_1 receptor were required for the inverse agonist activity that olmesartan exerts on GTPase-stimulating activity in a constitutively active AT_1-N111G mutant containing an Asn^{111} to Gly mutation.[9] However, studies using substituted cysteine accessibility mapping (SCAM) showed that conformation of the AT_1 receptor

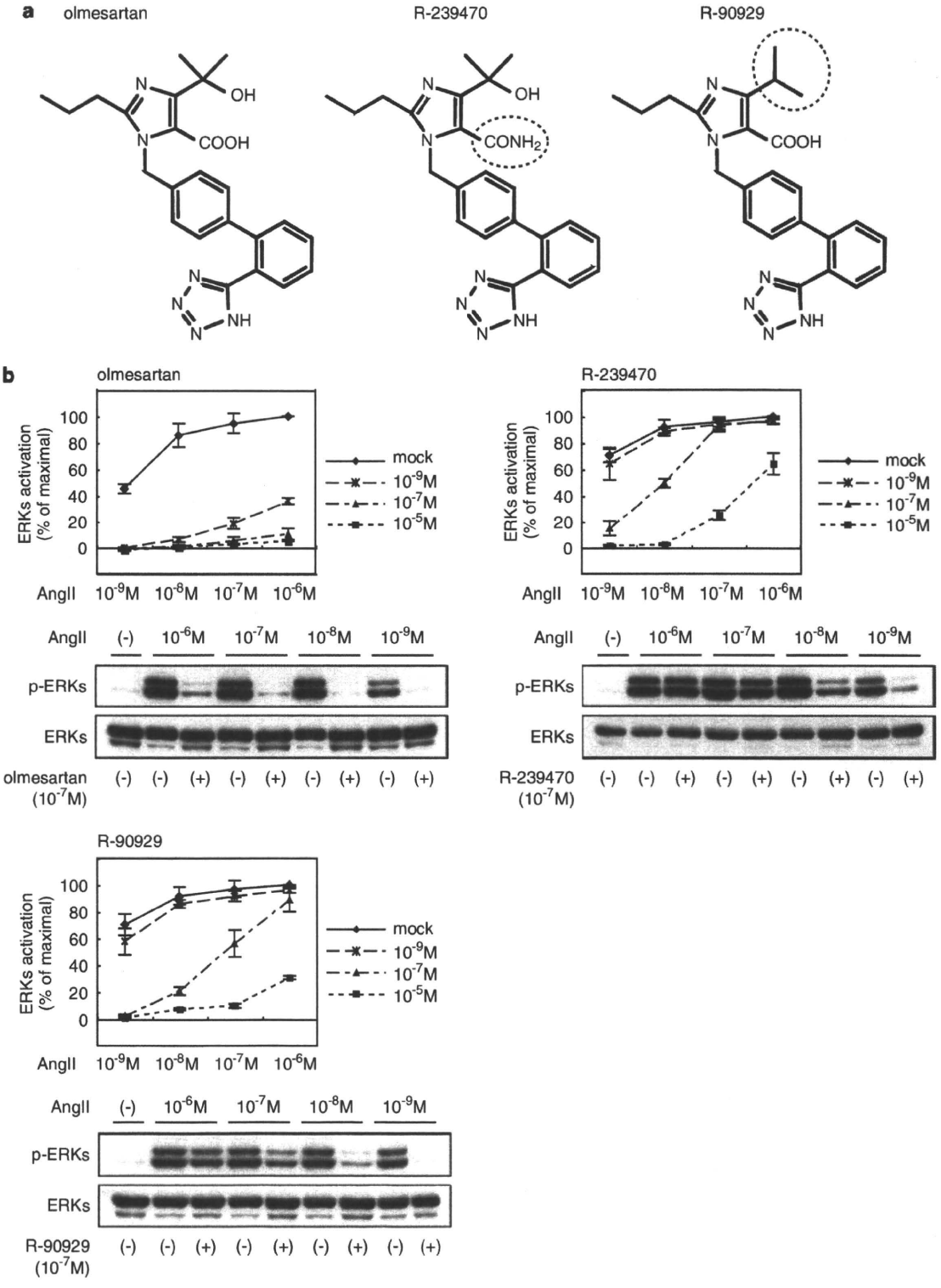

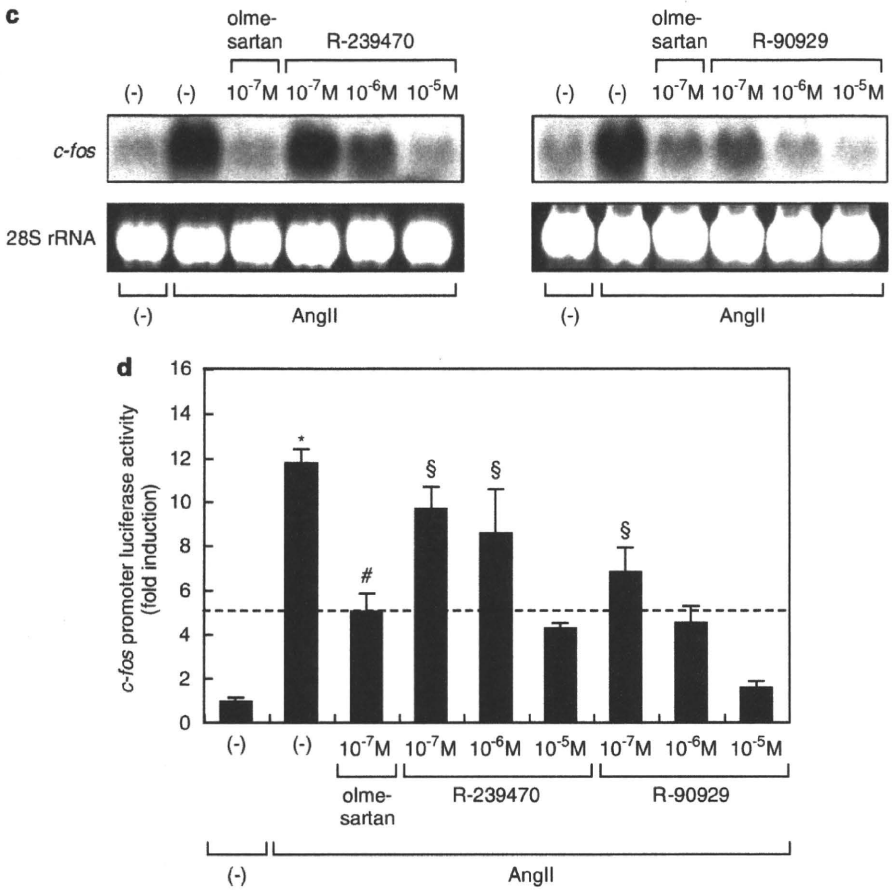

Figure 1 Continued.

during stretch-induced activation is quite different from that of the AT_1-N111G receptor.[7,10] Transmembrane domain 7 (TM7) of the AT_1 receptor undergoes a counterclockwise rotation and a shift toward the ligand-binding pocket in response to mechanical stretch,[7] but it shifts away from the ligand-binding pocket in the AT_1-N111G receptor.[10]

In this study, we show that, as an inverse agonist, olmesartan strongly inhibits the stretch-induced activation of the AT_1 receptor, as well as the constitutive activity of the AT_1-N111G receptor. In addition to the ternary interactions involving the hydroxyl group and the carboxyl group of the imidazole ring of olmesartan, a specific drug–receptor interaction between the tetrazole group of olmesartan and Gln^{257} of the AT_1 receptor is also important for the potent inverse agonist activity olmesartan exerts against stretch-induced AT_1 receptor activation. These results provide new insights into the structure–function relationship of AT_1 receptor inverse agonists.

METHODS

Materials

Olmesartan and its derivatives (R-88145, R-90929 and R-239470) were synthesized at the Research Laboratories of Daiichi Sankyo (Tokyo, Japan). The chemical structures of these compounds are shown in Figures 1a and 6b. AngII was purchased from Sigma-Aldrich (St Louis, MO, USA).

Cell culture and transfection

Cardiomyocytes obtained from ventricles of 1-day-old Wistar rats were plated at a field density of 1×10^5 cells per cm^2 on collagen-coated silicone rubber

Figure 1 The carboxyl group and the hydroxyl group are critical structural characteristics of olmesartan that lead to its insurmountable inhibition of angiotensin II (AT_1) receptors. (**a**) The chemical structures of olmesartan and its derivative compounds, R-239470 and R-90929, are shown. Olmesartan contains a carboxyl group and a hydroxyl group on its benzimidazole ring. R-239470 has a non-acidic carbamoyl group (circled $CONH_2$) instead of the carboxyl group, and R-90929 has no hydroxyl group (circled). (**b**) Response curves of AngII-mediated extracellular signal-regulated protein kinase (ERK) activation (upper panels). HEK293-AT_1 cells were pretreated with 10^{-7} M olmesartan, R-239470 or R-90929, and stimulated by AngII at indicated concentrations (lower panels). The activation of ERKs was determined using a polyclonal antibody against phosphorylated ERKs (p-ERKs). (**c**) The inhibitory effects of olmesartan and its derivative compounds, R-239470 and R-90929, on AngII-induced *c-fos* gene expression in HEK293 cells expressing the AT_1 receptor were examined by northern blot analysis of *c-fos* mRNA. (**d**) The inhibitory effects of olmesartan and its derivative compounds, R-239470 and R-90929, on AngII-induced *c-fos* gene expression in HEK293 cells expressing the AT_1 receptor were examined using a luciferase assay examining *c-fos* promoter activation. $^*P<0.01$ *vs.* that with no stimulation, $^{\#}P<0.01$ *vs.* that with AngII stimulation with no treatment, $^{\S}P<0.05$ *vs.* that with AngII stimulation with olmesartan (10^{-7} M) treatment.

dishes.[6] Cardiomyocytes and HEK293 cells were cultured in DMEM supplemented with 10% fetal bovine serum and nutrient-starved under serum-free conditions for 48 h before AngII or stretch stimulation. The expression vector for AT_1-WT and AT_1-mutant receptors[9] was transfected using FuGENE 6 Transfection Reagent (Roche Diagnostics, Basel, Switzerland) according to the manufacturer's instructions.[7]

Western blot analysis

Total cellular proteins (20 μg) were fractionated by SDS-PAGE and transferred to Hybond membranes (GE Healthcare, Piscataway, NJ, USA). The blotted membranes were incubated with a polyclonal antibody recognizing phospho-extracellular signal-regulated protein kinase 1/2 (ERK1/2) (Cell Signaling, Beverly, MA, USA) or ERK1/2 (Zymed Laboratories, South San Francisco, CA, USA). Horseradish peroxidase-conjugated anti-rabbit IgG (immunoglobulin G) antibody was used as secondary antibody, and signals were detected using the ECL detection kit (GE Healthcare).

RNA extraction and northern blot analysis

Total RNA was isolated from AT_1 receptor-transfected COS7 cells using an RNeasy Mini Kit (Qiagen, Valencia, CA, USA) according to the manufacturer's instructions, and 20 mg of total RNA was hybridized with a cDNA probe for *c-fos*.

Luciferase assay

The *c-fos* luciferase reporter plasmid, with or without the expression vector for the AT_1-WT or AT_1-N111G receptor, was transfected using FuGENE 6 Transfection Regent (Roche Diagnostics) according to the manufacturer's instructions. pRL-SV40 (Promega, Madison, WI, USA) was co-transfected as an internal control. Luciferase activity was measured 24 h after transfection using the Dual-Luciferase Reporter Assay System (Promega). Experiments were repeated at least in triplicate, and representative data are shown. The *c-fos* luciferase reporter plasmid was a generous gift from Dr M Tsuda (Toyama Medical and Pharmaceutical University, Toyama, Japan).

Statistical analysis

Statistical analyses comparing three or more independent experiments were carried out using one-way ANOVA (analysis of variance) and Dunnett's *t*-test. *P*-values < 0.05 were considered statistically significant.

RESULTS

Inhibitory effects of olmesartan and its derivative compounds on AngII-induced activation of the AT_1 receptor

We first determined the inhibitory effects of olmesartan and its derivative compounds, namely R-239470 and R-90929 (Figure 1a), on AngII-induced ERK activation. As previously reported, stimulation with AngII for 8 min induced a significant increase in the phosphorylation level of ERKs in HEK293 cells expressing the AT_1 receptor (Figure 1b).[7] Pretreatment with 10^{-7} M olmesartan strongly inhibited ERK activation induced even by 10^{-6} M AngII. The concentration–response curve of AngII-induced ERK activation in the presence of olmesartan (10^{-6} to 10^{-9} M) showed that olmesartan produced an insurmountable inhibitory effect on the AT_1 receptor, because it decreased the maximal response to AngII (Figure 1b). In contrast, R-239470 and R-90929, which lack the carboxyl or hydroxyl group possessed by olmesartan, respectively, showed surmountable inhibitory effects and led to a rightward shift of the concentration–response curve rather than a decrease in maximal response (Figure 1b).

We have further confirmed that these side-chain structures are crucial for the insurmountable inhibitory effect olmesartan exerts on AngII-induced *c-fos* gene expression. Stimulation with 10^{-6} M AngII significantly increased the expression level of *c-fos* mRNA, which was suppressed significantly by pretreatment with olmesartan but only partially by pretreatment with R-239470 or R-90929 (Figure 1c). Similarly, stimulation with 10^{-6} M AngII for 24 h induced a 12-fold increase in *c-fos* promoter activity, which was suppressed significantly by pretreatment with olmesartan but only partially suppressed by pretreatment with R-239470 or R-90929 (Figure 1d).

Collectively, these results suggest that the carboxyl group and the hydroxyl group on the imidazole ring of olmesartan are required for

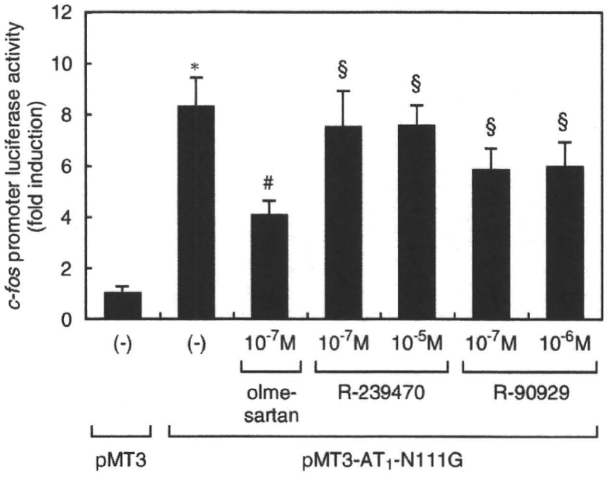

Figure 2 The carboxyl group and the hydroxyl group are critical structures in olmesartan's inverse agonist activity that allow it to suppress basal *c-fos* promoter activity. The basal activities of the AT_1-N111G mutant receptor were evaluated by a luciferase assay examining *c-fos* promoter activity in HEK293 cells expressing AT_1-N111G. Cells were treated with indicated concentrations of olmesartan, R-239470 or R-90929. $^*P<0.01$ *vs.* that of pMT3-transfected cells, $^{\#}P<0.01$ *vs.* that of untreated AT_1-N111G-transfected cells, $^{\S}P<0.05$ *vs.* that of AT_1-N111G-transfected cells treated with olmesartan (10^{-7} M). AT_1, angiotensin II type 1.

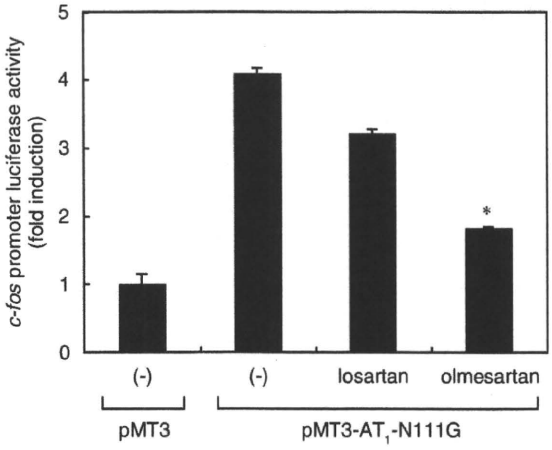

Figure 3 Comparison of the inverse agonist activities of olmesartan and losartan and their ability to suppress basal *c-fos* promoter activity. The basal activities of the AT_1-N111G mutant receptor were evaluated by a luciferase assay examining *c-fos* promoter activity in HEK293 cells expressing AT_1-N111G. The inhibitory effect of 10^{-7} M of olmesartan on basal *c-fos* promoter activity was much stronger than the inhibitory effect exerted by 10^{-7} M losartan. $^*P<0.01$ *vs.* that of losartan. AT_1, angiotensin II type 1.

the insurmountable inhibition of AngII-induced activation of the AT_1 receptor.

Inhibitory effects of olmesartan and its derivative compounds on stretch-induced ERK activation

A recent study showed that olmesartan suppresses the basal production of inositol phosphate (IP) in cells expressing WT AT_1 receptor (AT_1-WT) and a constitutively active mutant AT_1 receptor (AT_1-N111G).[9] We also found that basal *c-fos* promoter activity was suppressed by olmesartan in HEK293 cells expressing AT_1-N111G (Figure 2). The inhibitory effect of olmesartan on basal *c-fos* promoter activity was significantly stronger than that of losartan (Figure 3). Olmesartan is therefore defined as an inverse agonist of the AT_1 receptor because it decreases the basal activity level of the receptor in the absence of the agonist.

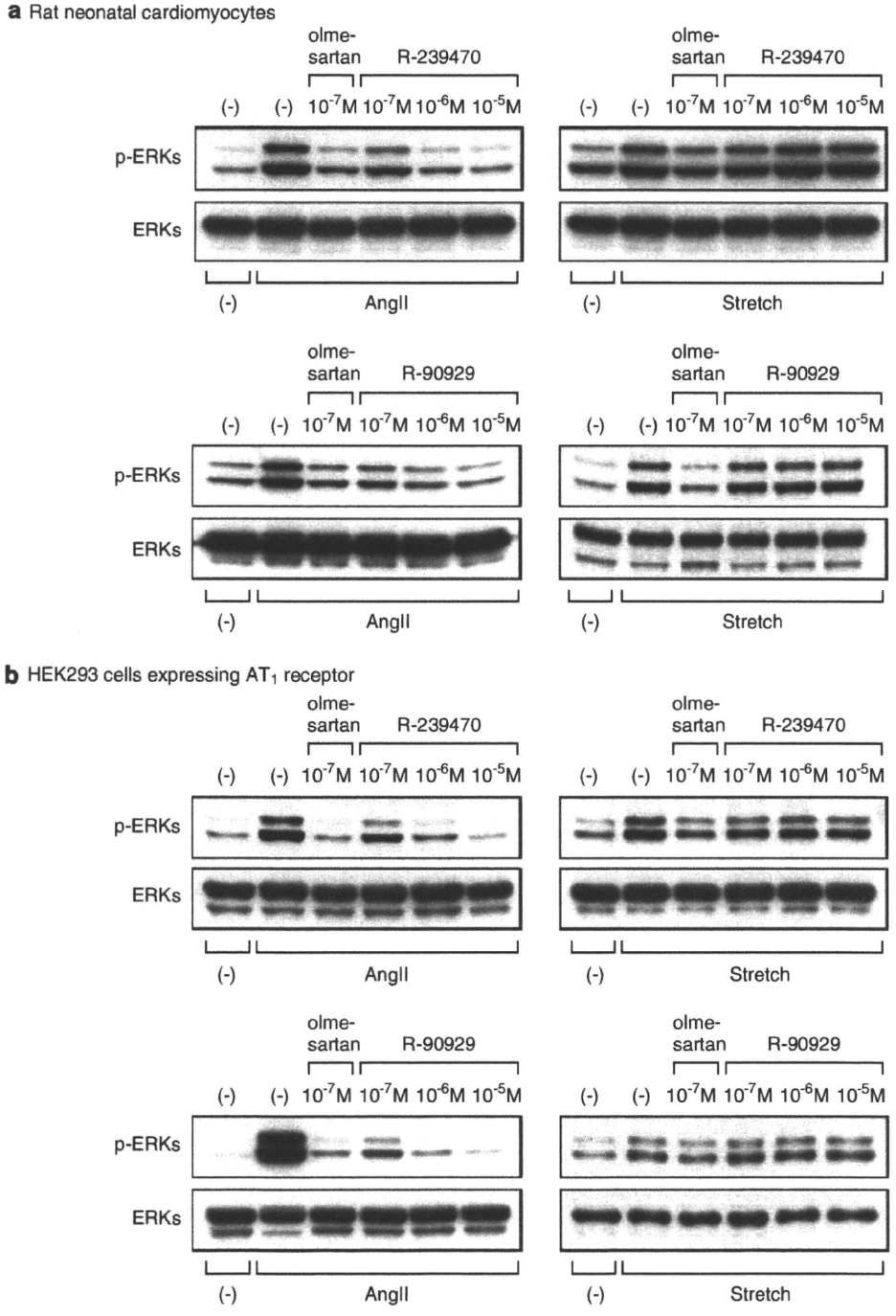

Figure 4 The carboxyl group and the hydroxyl group as critical structures for olmesartan's inverse agonist activity against stretch-induced ERK activation. Rat neonatal cardiomyocytes (**a**) or HEK293-AT_1 cells (**b**) were pretreated with indicated concentrations of olmesartan, R-239470 or R-90929, and stimulated by 10^{-7} M AngII (left) or by mechanical stretch (right). The activation of extracellular signal-regulated protein kinase (ERKs) was then determined. AT_1, angiotensin II type 1.

We recently reported that mechanical stress activates the AT_1 receptor independently of AngII and that this AngII-independent activation of AT_1 receptor is inhibited by the inverse agonist, candesartan.[6] Therefore, we next examined the inhibitory effects of olmesartan on stretch-induced ERK activation in cardiomyocytes cultured from neonatal rats. We found that the stretch-induced phosphorylation of ERKs in cultured cardiomyocytes was largely dependent on the direct activation of AT_1 receptor and that AngII, even if secreted from cardiomyocytes, had only a marginal role in the stretch-induced activation of ERKs.[6] We found that the activation of ERKs in response to mechanical stretch was significantly attenuated by a pretreatment with 10^{-7} M olmesartan (Figure 4a). Furthermore, to exclude the effect of secreted AngII on stretch-induced ERK activation, we imposed stretch stimulation on HEK293 cells that showed no detectable expression of angiotensinogen.[6] Neither stimulation with AngII nor mechanical stretch activated ERKs in HEK293 cells, but mechanical stretching did activate ERKs in these cells when the AT_1 receptor was overexpressed[6] (Figure 4b). Similar to the results in cardiomyocytes, pretreatment with olmesartan significantly inhibited stretch-induced ERK activation in HEK293 cells expressing the AT_1 receptor (HEK293-AT_1 cells) (Figure 4b). Furthermore, the inhibitory effect of olmesartan on stretch-induced ERK activation was significantly stronger than that of losartan (Figure 5). These results suggest that olmesartan, as a potent inverse agonist, strongly suppresses stretch-induced ERK activation, as well as the basal activity of the AT_1 receptor.

We further examined the inhibitory effects of R-239470 and R-90929 on stretch-induced ERK activation, both in cardiomyocytes and in HEK293-AT_1 cells. As shown in Figure 4, 10^{-7} M R-239470 or R-90929 could not inhibit ERK activation induced either by 10^{-7} M AngII or by mechanical stretch, although 10^{-7} M olmesartan inhibited ERK activation. Interestingly, AngII-induced ERK activation was inhibited by 10^{-5} M R-239470 and 10^{-6} M R-90929, but stretch-induced ERK activation was not inhibited by the same concentrations of these compounds (Figure 4). These results suggest that the carboxyl and the hydroxyl groups present in olmesartan are responsible for the potent inverse agonist activity olmesartan exerts against stretch-induced ERK activation. Similar to the results of experiments evaluating stretch-induced ERK activation, 10^{-5} M R-239470 and 10^{-6} M R-90929 failed to suppress basal *c-fos* promoter activity in HEK293 cells expressing AT_1-N111G (Figure 2).

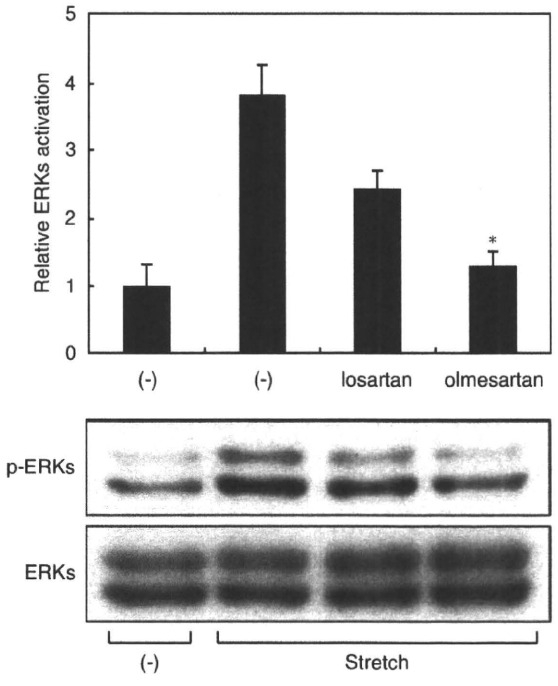

Figure 5 Comparison of the inverse agonist activities of olmesartan and losartan against stretch-induced ERK activation. HEK293-AT_1 cells were stimulated by mechanical stretch, and the activation of extracellular signal-regulated protein kinase (ERKs) was determined. The inhibitory effect of 10^{-7} M olmesartan on stretch-induced ERK activation was much stronger than that of 10^{-7} M losartan. *$P<0.01$ *vs.* that of losartan. AT_1, angiotensin II type 1.

Inhibitory effects of olmesartan on stretch-induced ERK activation in mutated AT_1 receptors

Structure–function analyses have shown that ternary interactions between the hydroxyl group of olmesartan and Tyr^{113} of the AT_1 receptor and between the carboxyl group of olmesartan and Lys^{199} and His^{256} of the AT_1 receptor are essential for the inverse agonist activity that olmesartan exerts on basal IP production in both AT_1-WT and AT_1-N111G receptors.[9] The tetrazole group of olmesartan also interacts with Gln^{257} of the AT_1 receptor, but its binding is not required to reduce the basal activity level of the AT_1 receptor.[9] We first examined the effect of olmesartan on stretch-induced ERK activation in HEK293 cells overexpressing AT_1-WT or an AT_1 mutant receptor harboring one of the following mutations: Y113F, K199Q, H256A or Q257A. As shown in Figure 6a, mechanical stretch-induced phosphorylation of ERKs occurred in AT_1-Y113F, AT_1-K199Q, AT_1-H256A and AT_1-Q257A cells in degrees equivalent to AT_1-WT cells. Interestingly, the inhibitory effects of olmesartan on stretch-induced ERK activation were abolished in cells expressing AT_1-Y113F, AT_1-K199Q, AT_1-H256A or AT_1-Q257A (Figure 6a). These results suggest that the interactions between olmesartan and Gln^{257}, Tyr^{113}, Lys^{199} and His^{256} are required for the potent inverse agonism olmesartan exerts on stretch-induced activation of the AT_1 receptor.

As the tetrazole ring of olmesartan interacts with Gln^{257} of the AT_1 receptor,[9] we next examined the inhibitory effect that R-88145 (in which the tetrazole group was replaced with a carboxyl group, Figure 6b) had on stretch-induced ERK activation in HEK293 cells overexpressing AT_1-WT. Although 10^{-7} M R-88145 did not inhibit ERK activation induced by 10^{-7} M AngII, 10^{-5} M R-88145 could inhibit ERK activation to an extent equivalent to 10^{-7} M olmesartan (Figure 6c). However, stretch-induced ERK activation was not significantly inhibited by 10^{-5} M R-88145 (Figure 6c). These results suggest that the interaction between the tetrazole group of olmesartan and Gln^{257} of the AT_1 receptor is also responsible for the potent inverse agonist activity olmesartan exerts against stretch-induced ERK activation.

DISCUSSION

The ARBs share a common mode of action, namely they block AngII-mediated responses, but the antihypertensive potency of ARBs differs by drug.[2,4] Indeed, the pharmacokinetics of ARBs in human bodies, specifically factors such as bioavailability, half-life duration and route of elimination, differ considerably between different ARBs. These different degrees of efficacy possessed by ARBs are based on differences in their chemical structures, which determine their unique pharmacological properties. Insurmountable antagonism is one of the pharmacological parameters that is relevant to antihypertensive efficacy.[11] Insurmountable antagonism reflects tight binding and a slow dissociation of the drug–receptor complex. ARBs with insurmountable

antagonist properties suppress maximal AngII-induced responses.[11] Recently, it was reported that olmesartan showed a higher degree of insurmountable antagonism than did telmisartan against AngII-induced IP accumulation in CHO-K1 cells expressing the AT_1 receptor.[12] In this study, we showed that olmesartan shows insurmountable antagonist activity against the AT_1 receptor and that the carboxyl and hydroxyl groups on the imidazole ring are required for the insurmountable inhibition of AngII-induced ERK activation and *c-fos* gene expression (Figure 1).

The unique side-chain structure olmesartan possesses (its carboxyl group and hydroxyl group) contributes to its specific receptor-binding activity. These drug–receptor interactions cooperate to stabilize the receptor in an inactive conformation and thereby confer inverse agonism against the basal expression of the *c-fos* gene (Figure 2) and the basal production of IP[9] in cells expressing the AT_1-N111G receptor, as well as insurmountable antagonism. The inverse agonist activities that ARBs exert against the constitutive activity of the AT_1 receptor could be an important pharmacological parameter that may be relevant to their efficacy at blood pressure lowering and in preventing end-organ damage. Although it remains unclear whether the subtle constitutive activity of the native AT_1 receptor has a pathophysiological role, the enhancement of its constitutive activity

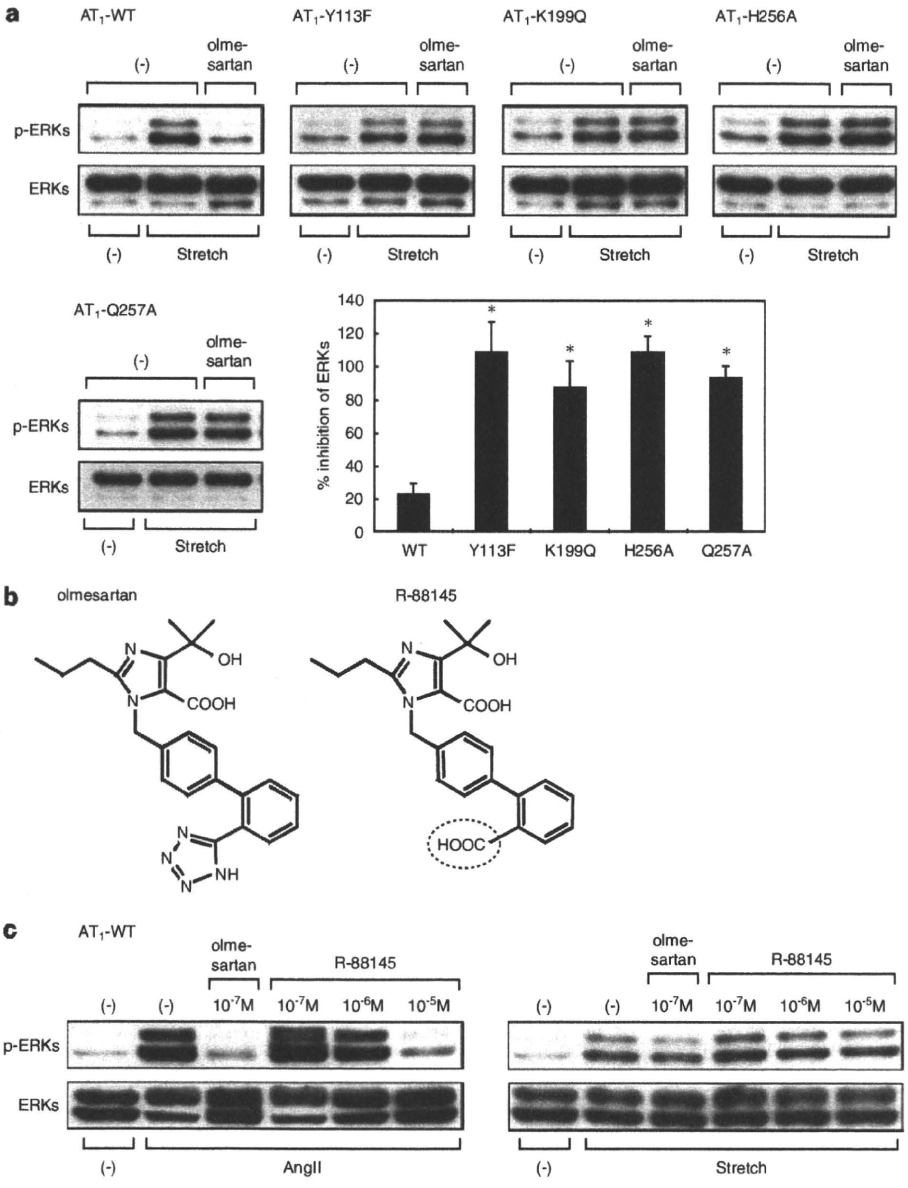

Figure 6 Specific drug–receptor interactions are required for olmesartan's inverse agonist activity against stretch-induced extracellular signal-regulated protein kinase (ERK) activation. (**a**) HEK293 cells expressing AT_1-WT, -Y113F, -K199Q, -H256A or -Q257A mutant receptors were pretreated with 10^{-7} M olmesartan and stimulated by mechanical stretch. The activation of ERKs was then determined. $^*P<0.01$ *vs.* that of wild-type AT_1-WT. (**b**) The chemical structures of olmesartan and R-88145, which has a carboxyl group (circled COOH) instead of a tetrazole group. (**c**) HEK293-AT_1 cells were pretreated with indicated concentrations of olmesartan or R-88145 and were stimulated by 10^{-7} M AngII (left) or mechanical stretch (right). The activation of ERKs was then determined. AT_1, angiotensin II type 1.

through upregulation of receptor expression may promote cardiovascular remodeling. Indeed, the expression level of the AT_1 receptor in vascular cells is upregulated by low-density lipoprotein cholesterol,[13] insulin,[14] glucose,[15] progesterone[16] and inflammatory cytokines, such as interleukin-1α or interleukin-6.[17,18] Analyses of the binding affinity of olmesartan for mutant AT_1 receptors as well as molecular modeling analyses indicated that the ternary interactions between the hydroxyl group and Tyr^{113} and between the carboxyl group and Lys^{199} and His^{256} are critical to the inverse agonist properties of olmesartan, but that the interaction between the tetrazole group and Gln^{257} is dispensable.[9] Interestingly, differential interactions between valsartan and Ser^{105}, and between Ser^{109} and Lys^{199}, are crucial for producing inverse agonism.[19] It has therefore been proposed that ARBs may bind to the AT_1 receptor primarily by docking at Lys^{199} and subsequently through a distinct combination of drug–receptor interactions in a drug-specific manner.[19] According to this model, the spatial pattern of drug–receptor contact points will determine the potency of the inverse agonist activity of a given ARB.

We recently showed that mechanical stretching of cells induces a counterclockwise rotation and a shift of TM7 of the AT_1 receptor toward the ligand-binding pocket.[7] However, TM7 shifts away from the ligand-binding pocket in the AT_1-N111G receptor,[10] implying that the conformation of AT_1 receptor during stretch-induced activation is different from that of the constitutively active AT_1 receptor. In general, GPCRs are structurally flexible and unstable, and multiple conformational states exist during the GPCR activation process.[20–22] In this study, we showed that, aside from the ternary drug–receptor interactions involving the hydroxyl and carboxyl groups of olmesartan, an additional interaction between the tetrazole group of olmesartan and Gln^{257} of the AT_1 receptor is required for its potent inverse agonism against stretch-induced AT_1 receptor activation (Figures 4 and 6). Each of the quaternary interactions involving the hydroxyl group, carboxyl group and tetrazole group contributes to a tight drug–receptor binding,[9] but is not sufficient enough to produce a potent inverse agonism against stretch-induced AT_1 receptor activation. Thus, the quaternary drug–receptor interactions work together to stabilize the receptor in an inactive conformation, even under conditions in which mechanical stretching occurs.

With regard to candesartan, the carboxyl group on the benzimidazole ring is responsible for its inverse agonism and leads to the suppression of both the constitutive activity and the mechanical stress-induced activation of the AT_1 receptor.[7] The SCAM studies showed that the binding of the carboxyl group of candesartan to Gln^{257} of TM6 and Thr^{287} of TM7 forcibly induces a clockwise rotation of TM6 and TM7, and leads to the stabilization of the AT_1 receptor in an inactive conformation.[7] At present, it remains unclear how the helical movement of TM7 induced by mechanical stretch is affected by the presence of olmesartan. According to molecular modeling, Thr^{287} of TM7 is located in a position that would allow it to form a hydrogen bond with His^{256} of TM6.[9] We assume that the helical movements of TM6 and TM7 are coupled and that TM7 may be restricted in motion when TM6 is rigidly bound to olmesartan through the dual interactions between the carboxyl group and His^{256} and between the tetrazole group of olmesartan and Gln^{257}.

Our study shows that olmesartan strongly inhibits both AngII-dependent and AngII-independent activation of the AT_1 receptor. Ternary drug–receptor interactions between the hydroxyl group and Tyr^{113} and between the carboxyl group and Lys^{199} and His^{256} are crucial for olmesartan's inverse agonist activity against the constitutive activity of an AT_1 mutant receptor, AT_1-N111G. In addition, a drug–receptor interaction between the tetrazole group of olmesartan and Gln^{257} of the AT_1 receptor is required for potent inverse agonism against stretch-induced AT_1 receptor activation. These results suggest that multivalent drug–receptor interactions cooperate in combination to stabilize the receptor in an inactive conformation according to the distinct processes of receptor activation. The inverse agonist activity of ARBs has therapeutic benefits in the prevention of load-induced cardiac hypertrophy,[5] and thus has the potential to affect long-term outcomes in patients with hypertension. Elucidation of the molecular basis for the inverse agonist activity of ARBs in relation to their chemical structure will help to categorize ARBs according to their individual efficacies in receptor inactivation and will also help researchers to develop novel ARBs with superb efficacy in terms of blood pressure lowering and end-organ protection.

CONFLICT OF INTEREST

The authors declare no conflict of interest.

ACKNOWLEDGEMENTS

We thank A Furuyama, M Ikeda, Y Ohtsuki and I Sakamoto for their excellent technical assistance. This work was supported in part by grants from the Japanese Ministry of Education, Science, Sports, and Culture, as well as Health and Labor Sciences Research Grants (to IK and HA). Additional grants from the Japan Intractable Diseases Research Foundation, the Kowa Life Science Foundation and the Takeda Science Foundation (to HA) were used to support this research.

1 de Gasparo M, Catt KJ, Inagami T, Wright JW, Unger T. International union of pharmacology. XXIII. The angiotensin II receptors. *Pharmacol Rev* 2000; **52**: 415–472.
2 Zaman MA, Oparil S, Calhoun DA. Drugs targeting the renin-angiotensin-aldosterone system. *Nat Rev Drug Discov* 2002; **1**: 621–636.
3 Kjeldsen SE, Dahlof B, Devereux RB, Julius S, Aurup P, Edelman J, Beevers G, de Faire U, Fyhrquist F, Ibsen H, Kristianson K, Lederballe-Pedersen O, Lindholm LH, Nieminen MS, Omvik P, Oparil S, Snapinn S, Wedel H. Effects of losartan on cardiovascular morbidity and mortality in patients with isolated systolic hypertension and left ventricular hypertrophy: a Losartan Intervention for Endpoint Reduction (LIFE) substudy. *JAMA* 2002; **288**: 1491–1498.
4 Oparil S. Newly emerging pharmacologic differences in angiotensin II receptor blockers. *Am J Hypertens* 2000; **13**: 18S–24S.
5 Akazawa H, Yasuda N, Komuro I. Mechanisms and functions of agonist-independent activation in the angiotensin II type 1 receptor. *Mol Cell Endocrinol* 2009; **302**: 140–147.
6 Zou Y, Akazawa H, Qin Y, Sano M, Takano H, Minamino T, Makita N, Iwanaga K, Zhu W, Kudoh S, Toko H, Tamura K, Kihara M, Nagai T, Fukamizu A, Umemura S, Iiri T, Fujita T, Komuro I. Mechanical stress activates angiotensin II type 1 receptor without the involvement of angiotensin II. *Nat Cell Biol* 2004; **6**: 499–506.
7 Yasuda N, Miura S, Akazawa H, Tanaka T, Qin Y, Kiya Y, Imaizumi S, Fujino M, Ito K, Zou Y, Fukuhara S, Kunimoto S, Fukuzaki K, Sato T, Ge J, Mochizuki N, Nakaya H, Saku K, Komuro I. Conformational switch of angiotensin II type 1 receptor underlying mechanical stress-induced activation. *EMBO Rep* 2008; **9**: 179–186.
8 Milligan G. Constitutive activity and inverse agonists of G protein-coupled receptors: a current perspective. *Mol Pharmacol* 2003; **64**: 1271–1276.
9 Miura S, Fujino M, Hanzawa H, Kiya Y, Imaizumi S, Matsuo Y, Tomita S, Uehara Y, Karnik SS, Yanagisawa H, Koike H, Komuro I, Saku K. Molecular mechanism underlying inverse agonist of angiotensin II type 1 receptor. *J Biol Chem* 2006; **281**: 19288–19295.
10 Boucard AA, Roy M, Beaulieu ME, Lavigne P, Escher E, Guillemette G, Leduc R. Constitutive activation of the angiotensin II type 1 receptor alters the spatial proximity of transmembrane 7 to the ligand-binding pocket. *J Biol Chem* 2003; **278**: 36628–36636.
11 Van Liefde I, Vauquelin G. Sartan-AT(1) receptor interactions: in vitro evidence for insurmountable antagonism and inverse agonism. *Mol Cell Endocrinol* 2009; **302**: 237–243.
12 Le MT, Pugsley MK, Vauquelin G, Van Liefde I. Molecular characterisation of the interactions between olmesartan and telmisartan and the human angiotensin II AT1 receptor. *Br J Pharmacol* 2007; **151**: 952–962.
13 Nickenig G, Jung O, Strehlow K, Zolk O, Linz W, Scholkens BA, Bohm M. Hypercholesterolemia is associated with enhanced angiotensin AT1-receptor expression. *Am J Physiol* 1997; **272**: H2701–H2707.

14 Nickenig G, Roling J, Strehlow K, Schnabel P, Bohm M. Insulin induces upregulation of vascular AT1 receptor gene expression by posttranscriptional mechanisms. *Circulation* 1998; **98**: 2453–2460.
15 Sodhi CP, Kanwar YS, Sahai A. Hypoxia and high glucose upregulate AT1 receptor expression and potentiate ANG II-induced proliferation in VSM cells. *Am J Physiol Heart Circ Physiol* 2003; **284**: H846–H852.
16 Nickenig G, Strehlow K, Wassmann S, Baumer AT, Albory K, Sauer H, Bohm M. Differential effects of estrogen and progesterone on AT(1) receptor gene expression in vascular smooth muscle cells. *Circulation* 2000; **102**: 1828–1833.
17 Sasamura H, Nakazato Y, Hayashida T, Kitamura Y, Hayashi M, Saruta T. Regulation of vascular type 1 angiotensin receptors by cytokines. *Hypertension* 1997; **30**: 35–41.
18 Wassmann S, Stumpf M, Strehlow K, Schmid A, Schieffer B, Bohm M, Nickenig G. Interleukin-6 induces oxidative stress and endothelial dysfunction by overexpression of the angiotensin II type 1 receptor. *Circ Res* 2004; **94**: 534–541.
19 Miura S, Kiya Y, Kanazawa T, Imaizumi S, Fujino M, Matsuo Y, Karnik SS, Saku K. Differential bonding interactions of inverse agonists of angiotensin II type 1 receptor in stabilizing the inactive state. *Mol Endocrinol* 2008; **22**: 139–146.
20 Gether U. Uncovering molecular mechanisms involved in activation of G protein-coupled receptors. *Endocr Rev* 2000; **21**: 90–113.
21 Miura S, Saku K, Karnik SS. Molecular analysis of the structure and function of the angiotensin II type 1 receptor. *Hypertens Res* 2003; **26**: 937–943.
22 Perez DM, Karnik SS. Multiple signaling states of G-protein-coupled receptors. *Pharmacol Rev* 2005; **57**: 147–161.

Journal of Molecular and Cellular Cardiology 47 (2009) 698–705

Contents lists available at ScienceDirect

Journal of Molecular and Cellular Cardiology

journal homepage: www.elsevier.com/locate/yjmcc

Original article

Chronic doxorubicin cardiotoxicity is mediated by oxidative DNA damage-ATM-p53-apoptosis pathway and attenuated by pitavastatin through the inhibition of Rac1 activity

Masashi Yoshida [a], Ichiro Shiojima [a,b], Hiroyuki Ikeda [a], Issei Komuro [a,b,*]

[a] Department of Cardiovascular Science and Medicine, Chiba University Graduate School of Medicine, 1-8-1 Inohana, Chuo-ku, Chiba, 260-8670, Japan
[b] Department of Cardiovascular Medicine, Osaka University Graduate School of Medicine, 2-2 Yamadaoka, Suita 565-0871, Japan

ARTICLE INFO

Article history:
Received 20 May 2009
Received in revised form 8 July 2009
Accepted 27 July 2009
Available online 3 August 2009

Keywords:
Doxorubicin
Cardiomyopathy
p53
Apoptosis
Statins

ABSTRACT

Doxorubicin is known to have cumulative dose-dependent cardiotoxicity, and a tumor suppressor protein p53 has been implicated in the pathogenesis of doxorubicin cardiotoxicity. However, how p53 is induced by doxorubicin and mediates the cardiotoxic effects of doxorubicin remains elusive. In cultured cardiac myocytes, doxorubicin induced oxidative stress, DNA damage, ATM activation, and p53 induction. A free radical scavenger NAC attenuated all of these events, whereas an ATM kinase inhibitor wortmannin attenuated doxorubicin-induced ATM activation and p53 induction but not oxidative stress. Doxorubicin treatment in vivo also induced oxidative stress, DNA damage, ATM activation, and p53 accumulation. These observations suggest that p53 induction by doxorubicin is mediated by oxidative DNA damage-ATM pathway. Doxorubicin-induced contractile dysfunction and myocyte apoptosis in vivo were attenuated in heterozygous p53 deficient mice and cardiac-restricted Bcl-2 transgenic mice, suggesting that myocyte apoptosis plays a central role downstream of p53 in doxorubicin cardiotoxicity. We also tested whether pitavastatin exerts protective effects on doxorubicin cardiotoxicity. Pitavastatin attenuated doxorubicin-induced oxidative stress, DNA damage, ATM activation, p53 accumulation, and apoptosis in vitro. Pitavastatin also attenuated myocyte apoptosis and contractile dysfunction in vivo. The beneficial effects of pitavastatin were reversed by intermediate products of the mevalonate pathway that are required for the activation of Rac1, and Rac1 inhibitor exhibited cardioprotective effects comparable to those of pitavastatin. These data collectively suggest that doxorubicin-induced cardiotoxicity is mediated by oxidative DNA damage-ATM-p53-apoptosis pathway, and is attenuated by pitavastatin through its antioxidant effect involving Rac1 inhibition.

1. Introduction

Doxorubicin is a potent chemotherapeutic agent used for a wide variety of malignancies. However, the use of doxorubicin is limited due to its cumulative dose-dependent cardiotoxicity, which sometimes results in doxorubicin cardiomyopathy [1,2]. Although the precise mechanism of doxorubicin-induced cardiotoxicity is not completely understood, oxidative stress has been proposed as one of the mechanisms of cardiotoxicity by doxorubicin. Acute or chronic doxorubicin cardiotoxicity is reduced in transgenic mice overexpressing mitochondrial MnSOD or cysteine-rich metallothioneins, respectively [3,4], supporting the idea that oxidative stress mediates doxorubicin cardiotoxicity. It has also been suggested that a tumor suppressor protein p53 is a critical mediator of doxorubicin cardiotoxicity. This notion is supported by the observation that doxorubicin induces p53 accumulation in the heart and that either pharmacological or genetic ablation of p53 results in the attenuation of cardiotoxicity following doxorubicin treatment [5,6]. However, how p53 is activated in the heart by doxorubicin or how p53 mediates the cardiotoxic effects of doxorubicin remains elusive. Although myocyte apoptosis induced by doxorubicin was attenuated by p53 ablation [5,6], this does not directly demonstrate the causative role of cardiomyocyte apoptosis in doxorubicin-mediated cardiotoxicity. It was recently shown that p53 inhibits hypoxia-inducible factor-1 (Hif-1) and thereby promotes myocardial ischemia [7]. More recently, p53-dependent inhibition of mammalian target of rapamycin (mTOR) was proposed as a mechanism of acute doxorubicin cardiotoxicity independently of p53-induced apoptosis [8]. Thus, it is possible that p53-dependent but apoptosis-independent mechanisms also contribute to the pathogenesis of doxorubicin cardiotoxicity.

The 3-hydroxy-3-methylglutaryl-CoA (HMG-CoA) reductase inhibitors or statins are widely used as a cholesterol lowering drug, and also known to be cardioprotective through lipid lowering-independent pleiotropic effects [9]. For instance, statin treatment protects against

* Corresponding author. Department of Cardiovascular Science and Medicine, Chiba University Graduate School of Medicine, 1-8-1 Inohana, Chuo-ku, Chiba, 260-8670, Japan.
E-mail address: komuro-tky@umin.ac.jp (I. Komuro).

0022-2828/$ – see front matter © 2009 Elsevier Inc. All rights reserved.
doi:10.1016/j.yjmcc.2009.07.024

stroke, ischemia–reperfusion injury, cardiac hypertrophy, and heart failure in normocholesterolemic animals [10–13]. Most of these pleiotropic effects are thought to be mediated by inhibiting the synthesis of isoprenoid intermediates such as farnesyl pyrophosphate (FPP) and geranylgeranyl pyrophosphate (GGPP) downstream of the mevalonate pathway [9]. FPP and GGPP serve as lipid attachments for the post-translational modifications of a variety of proteins including small G proteins. Of note, activation of NADPH oxidase requires geranylgeranylation of Rac1 [14], and it was shown that the protective effect of statins against cardiac hypertrophy is mediated by its antioxidant effects involving the inhibition of Rac1 activity [12]. Whether statins exert protective effects against doxorubicin cardiotoxicity by similar mechanisms remains unknown.

In this study we explored how p53 accumulation is induced by doxorubicin and how p53 mediates the cardiotoxic effects of doxorubicin. We also examined the potential mechanisms of cardioprotection by statins against doxorubicin. We show that doxorubicin cardiotoxicity is mediated by oxidative DNA damage-ATM-p53-apoptosis pathway and attenuated by pitavastatin through the inhibition of Rac1 activity.

2. Materials and methods

2.1. Reagents

Doxorubicin was from Kyowa Hakko Kogyo (Tokyo, Japan). N-acetyl-L-cysteine (NAC), mevalonolactone, farnesyl pyrophosphate (FPP), geranylgeranyl pyrophosphate (GGPP), NADPH, and lucigenin were from Sigma (St. Louis, Missouri). Wortmannin, farnesyltransferase inhibitor (FTI (FTI-276)), geranylgeranyl transferase inhibitor (GTI (GTI-286)), Rac1 inhibitor (NSC23766), and apocynin were from Calbiochem (San Diego, California). Dihydroethidium (DHE) and 5-(and-6)-chloromethyl-2′, 7′-dichlorodihydrofluorescein diacetate, acetyl ester (CM-H2DCFDA) were from Molecular Probes (Eugene, Oregon). Hydrogen peroxide (H_2O_2) was from Wako (Osaka, Japan). Pitavastatin was provided by Kowa (Tokyo, Japan).

2.2. Cell culture and treatment

Neonatal rat cardiomyocytes were prepared as previously described [15]. Doxorubicin (1 μM) was added to culture media 24 h after myocyte preparation. Where indicated, cells were pretreated for 30 min with the following compounds: wortmannin, 1–50 μM; NAC, 1–50 μM; pitavastatin, 0.1–10 μM; mevalonate, 200 μM; GGPP, 10 μM; FPP, 10 μM; GTI, 30 μM; FTI, 20 nM; Rac1 inhibitor, 100 μM.

2.3. Animal models

C57BL/6 mice were purchased from SLC (Shizuoka, Japan). Heterozygous p53 deficient mice on C57BL/6 background were from Jackson Laboratory (Bar Harbar, Maine). For experiments using p53 heterozygous knockout mice, C57BL/6 mice were used as controls. Generation and genotyping of transgenic mice with cardiac-restricted overexpression of human Bcl-2 have been previously described [16]. Bcl-2 transgenic mice were on mixed background and their non-transgenic littermates were used as controls. Doxorubicin treatment was performed with intraperitoneal injection of doxorubicin (6 mg/kg) once a week for 4 weeks. Pitavastatin (3 mg/kg) treatment was performed with daily oral administration. All animal procedures were performed with the approval of the Institutional Animal Care and Use Committee of Chiba University.

2.4. Echocardiography

Transthoracic echocardiography was performed with Vevo 660 (VISUAL SONIC, Ontario, Canada) equipped with a 25-MHz imaging transducer. All recordings were performed on conscious animals.

2.5. Oxidative stress detection

Total intracellular oxidation in cultured cardiomyocytes was assessed with 2′, 7′-dichlorofluorescein (DCF) fluorescence using CM-H2DCFDA. Intracellular oxidative stress was monitored by microscopic observation and measurement of intracellular fluorescence intensity using the Mithras LB940 (Berthold, Germany) as previously described [17]. Measurements were carried out for 5 samples in each group according to the manufacturer's instruction. Histological detection of superoxide production was assessed with DHE as previously described [18].

2.6. DNA damage detection

To assess DNA damage in cultured cardiomyocytes, CometAssay (Trevigen, Gaithersburg, MD, USA) was performed according to the manufacturer's instruction. During electrophoresis, undamaged DNA remains within the confines of the nucleus, whereas damaged DNA migrates out of the nucleus in the shape of a comet. Each comet was assigned a value of 0 (no tail) to 4 (almost all DNA in tail), and 100 cells per slide and 3 slides per treatment were analyzed. To assess DNA damage in the heart in vivo, paraffin sections of the heart samples fixed in 10% formalin were stained with an antibody against phosphorylated histone H2AX (γH2AX) (Cell Signaling Technology, Beverly, Massachusetts) and dystrophin (Novocastra Laboratories, Newcastle, UK).

2.7. Western blot analysis

Western blot analysis was performed as previously described [7]. Unless mentioned otherwise, whole cell or tissue lysates were used for analysis. For Rac1 subcellular localization assay, membrane and cytosolic proteins were prepared using proteoextract native membrane protein extraction kit (Calbiochem) according to the manufacturer's instruction. Specific signals were detected using enhanced chemiluminescence (Amersham, Buckinghamshire, UK). The primary antibodies used for western blotting were as follows: phospho-ATM (S1981) (Rockland, Philadelphia, Pennsylvania), ATM (Santa Cruz Biotechnology), phospho-p53 (S15) (Santa Cruz Biotechnology), p53 (Cell Signaling Technology), Bax (Santa Cruz Biotechnology), cleaved caspase-3 (Cell Signaling Technology), Rac1 (Santa Cruz Biotechnology), and actin (Sigma).

2.8. NADPH oxidase assay

NADPH oxidase activity was measured as previously described [19]. All measurements were performed as triplicates in 96-well luminometer plates.

2.9. Cell death assay

The number of viable cells in vitro was determined with trypan blue exclusion method [20]. For apoptosis analysis in vitro and in vivo, TUNEL labeling was performed according to the manufacturer's protocol (In Situ Apoptosis Detection Kit; Takara, Shiga, Japan). TUNEL-positive cells were counted in 3 randomly selected low-power fields from each culture dish, 3 dishes for each group in vitro. TUNEL/dystrophin double positive cells were counted in 20 randomly selected high-power fields from each heart sample in vivo.

2.10. Statistical analysis

All values are expressed as means ± SEM. Multiple group comparison was performed by one-way ANOVA followed by the Tukey's HSD for comparison of means. Comparisons between two groups were analyzed by two-way ANOVA. Data processing and analysis were performed by using JMP version 5.1 (Statical Analysis

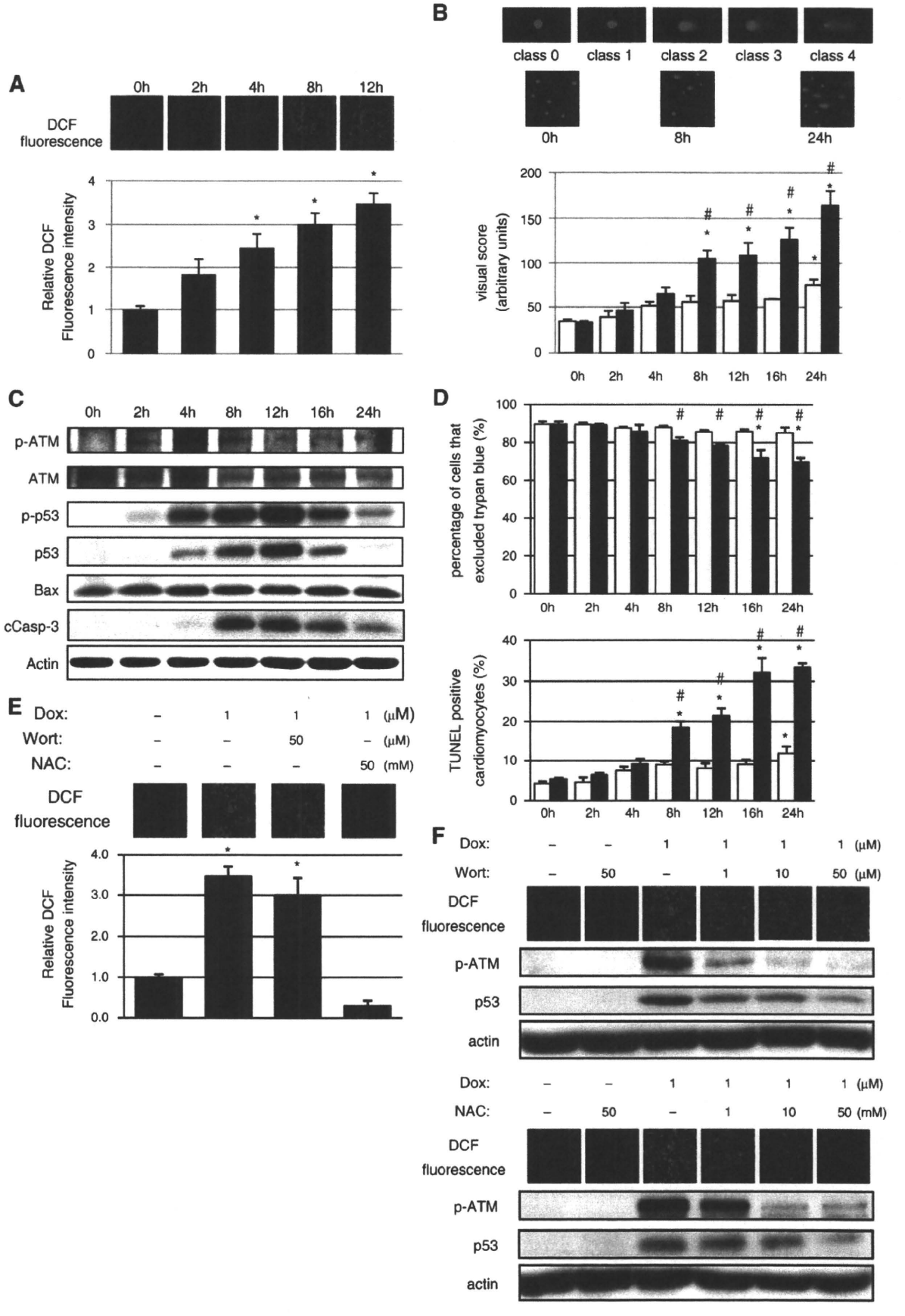
A
0h 2h 4h 8h 12h
DCF fluorescence
Relative DCF Fluorescence intensity
B
class 0 class 1 class 2 class 3 class 4
0h 8h 24h
visual score (arbitrary units)
0h 2h 4h 8h 12h 16h 24h
C
0h 2h 4h 8h 12h 16h 24h
p-ATM
ATM
p-p53
p53
Bax
cCasp-3
Actin
D
percentage of cells that excluded trypan blue (%)
TUNEL positive cardiomyocytes (%)
0h 2h 4h 8h 12h 16h 24h
E
Dox: – 1 1 1 (μM)
Wort: – – 50 – (μM)
NAC: – – – 50 (mM)
DCF fluorescence
Relative DCF Fluorescence intensity
F
Dox: – – 1 1 1 1 (μM)
Wort: – 50 – 1 10 50 (μM)
DCF fluorescence
p-ATM
p53
actin
Dox: – – 1 1 1 1 (μM)
NAC: – 50 – 1 10 50 (mM)
DCF fluorescence
p-ATM
p53
actin

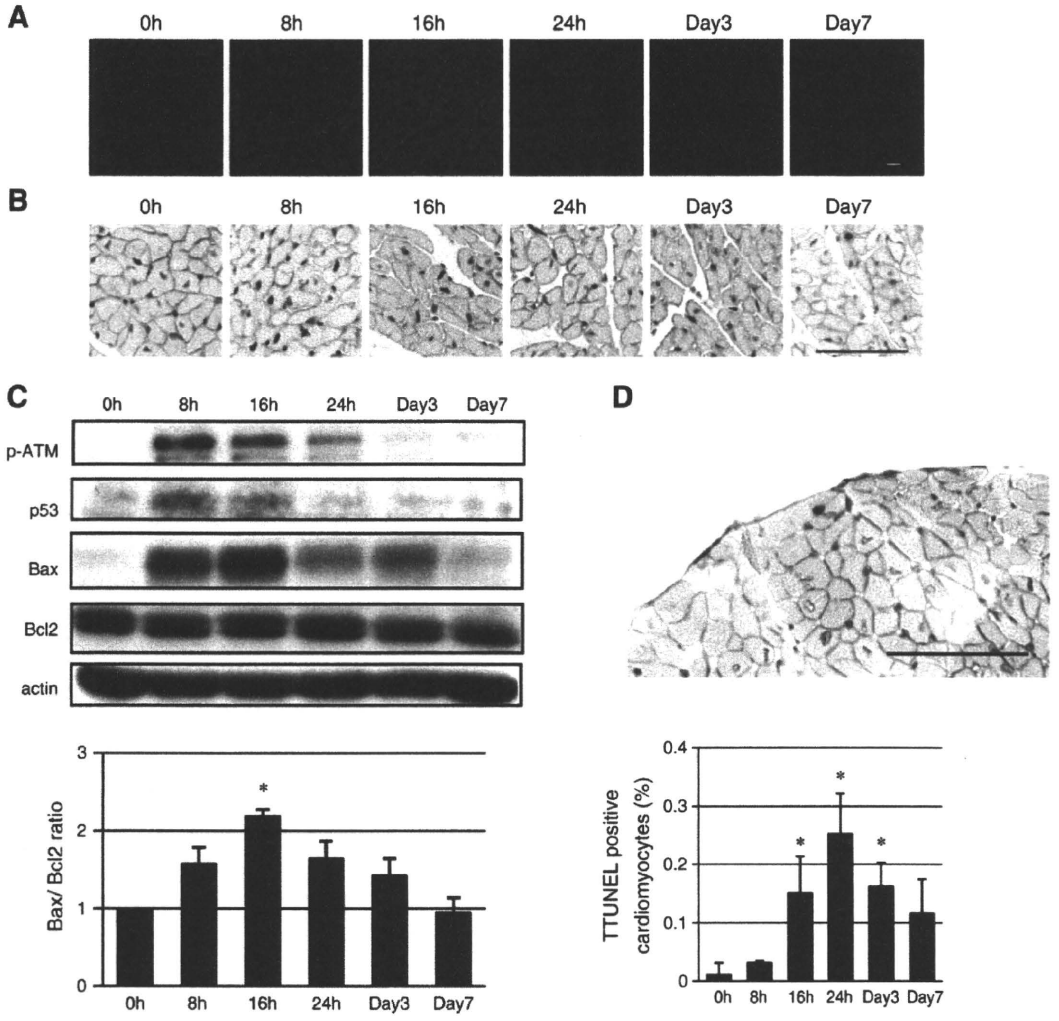

Fig. 2. Doxorubicin induces oxidative DNA damage, ATM kinase activation, and p53 accumulation in the heart in vivo. (A) Doxorubicin-induced oxidative stress in vivo. Oxidative stress was assessed by DHE assay. (B) Doxorubicin-induced DNA damage in vivo. DNA damage was assessed by γH2AX staining. (C) Doxorubicin-induced ATM activation, p53 accumulation, and cardiomyocyte apoptosis in vivo. Left: Western blot analysis. Molecular weight of Bcl2 is 26 kDa. Right: quantification of Bax/Bcl2 ratio. *$P<0.05$ vs 0 h. (D) Doxorubicin-induced cardiomyocyte apoptosis as assessed by TUNEL staining. Left: double-immunostaining for TUNEL (brown) and dystrophin (red) in the heart after doxorubicin treatment. Scale bar, 100 μm. Right: time course of the number of TUNEL-positive cardiomyocytes. *$P<0.05$ vs 0 h.

Systems). Values of $P<0.05$ were considered to be statistically significant.

3. Results

3.1. Doxorubicin induces p53 accumulation in cardiac myocytes via oxidative DNA damage-ATM pathway

Previous studies implicated oxidative stress and p53 accumulation in doxorubicin cardiotoxicity [1,2]. Because DNA damage links oxidative stress to p53 accumulation [21,22], we tested whether DNA damage response mediates doxorubicin cardiotoxicity in cultured cardiac myocytes. Doxorubicin treatment induced oxidative stress and DNA damage in cardiac myocytes, as assessed by DCF fluorescence and CometAssay. Statistically significant increase in DCF fluorescence and DNA damage was observed from 4 h and 8 h after doxorubicin treatment, respectively (Figs. 1(A) and (B)). Increased oxidative stress and DNA damage was associated with an increase in phospho-ATM (ataxia telangiectasia mutated) levels, p53 accumulation, and

Fig. 1. Doxorubicin induces p53 accumulation in cardiac myocytes through oxidative DNA damage-ATM pathway. (A) Doxorubicin-induced oxidative stress. Top: DCF fluorescence. Bottom: quantification of DCF fluorescence. *$P<0.05$ vs 0 h. (B) Doxorubicin-induced DNA damage as assessed by CometAssay. Top: classification of comets from 0 (no tail) to 4 (almost all DNA in tail). Middle: representative pictures of CometAssay at indicated time points. Bottom: time course of visual scores. White columns and black columns represent control (saline-treated) group and doxorubicin-treated group, respectively. *$P<0.05$ vs control group at 0 h; #$P<0.05$ vs control group at the same time points. (C) Doxorubicin-induced ATM activation, p53 accumulation, and cardiomyocyte apoptosis as assessed by Western blot analysis. cCasp-3, cleaved caspase-3. Molecular weights of the proteins are 370 kDa for pATM/ATM, 53 kDa for p-p53/p53, 23 kDa for Bax, 19 kDa for cleaved caspase-3, and 42 kDa for actin. (D) Doxorubicin-induced cardiomyocyte death. Top: trypan blue exclusion assay. White columns and black columns represent control (saline-treated) group and doxorubicin-treated group, respectively. *$P<0.05$ vs control group at 0 h; #$P<0.05$ vs control group at the same time points. Bottom: TUNEL assay. White columns and black columns represent control (saline-treated) group and doxorubicin-treated group, respectively. *$P<0.05$ vs control group at 0 h; #$P<0.05$ vs control group at the same time points. (E) NAC but not wortmannin attenuates doxorubicin-induced oxidative stress. Top: DCF fluorescence. Bottom: quantification of DCF fluorescence. *$P<0.05$ vs 0 h. (F) Both NAC and wortmannin attenuates doxorubicin-induced ATM activation and p53 accumulation. DCF fluorescence, ATM, and phospho-p53 were assessed 12 h, 4 h, and 12 h after doxorubicin treatment, respectively. Wort, wortmannin.

apoptotic cell death (Figs. 1(C) and (D)). Definitive increases in phospho-ATM and phospho-p53 were observed from 4 h after doxorubicin treatment, followed by cleaved Caspase-3 expression and apoptotic cell death from 8 h after doxorubicin treatment. This is consistent with the notion that p53 phosphorylation by ATM results in p53 stabilization, leading to apoptotic cell death. Doxorubicin-induced oxidative stress was attenuated by a free radical scavenger NAC but not by an ATM kinase inhibitor wortmannin, whereas doxorubicin-induced p53 accumulation was reduced both by NAC and wortmannin (Figs. 1(E) and (F)), indicating that ATM is situated downstream of oxidative stress in doxorubicin-induced p53 accumulation. We also checked the involvement of oxidative DNA damage-ATM pathway in doxorubicin cardiotoxicity in vivo. Single intra-peritoneal injection of doxorubicin (6 mg/kg) induced oxidative stress and DNA damage as assessed by DHE assay and γH2AX staining, respectively (Figs. 2(A) and (B)). Doxorubicin-induced oxidative stress and DNA damage in the heart were associated with a transient increase in

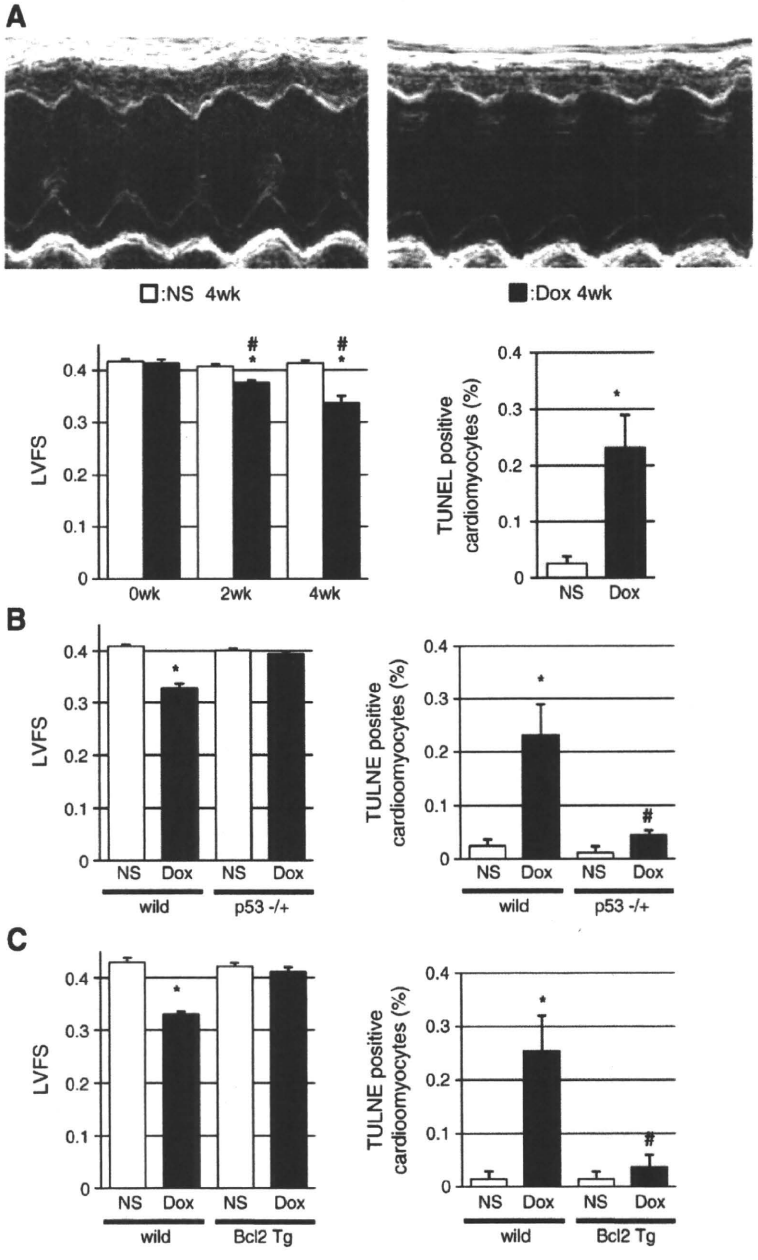

Fig. 3. Doxorubicin cardiotoxicity is mediated by p53-dependent cardiomyocyte apoptosis. (A) Doxorubicin-induced cardiomyopathy in wild type mice. Top: representative echocardiograms of the heart treated with normal saline (NS) or doxorubicin (Dox: 6 mg/kg) once a week for 4 weeks. Bottom left: left ventricular fractional shortening of mice treated with normal saline (white columns) or doxorubicin (black columns). *$P<0.05$ vs 0 week; #$P<0.05$ vs normal saline-treated group at the same time point. Bottom right: number of TUNEL-positive cardiomyocytes 4 weeks after doxorubicin treatment. *$P<0.05$ vs normal saline (NS)-treated group. (B) Doxorubicin-induced cardiomyopathy is attenuated in heterozygous p53 deficient mice. Left: left ventricular fractional shortening of mice treated with normal saline (NS) or doxorubicin (Dox). Right: number of TUNEL-positive cardiomyocytes 4 weeks after doxorubicin treatment. *$P<0.05$ vs saline-treated wild type mice; #$P<0.05$ vs doxorubicin-treated wild type mice. (C) Doxorubicin-induced cardiomyopathy is attenuated in cardiac-specific Bcl-2 transgenic mice. Left: left ventricular fractional shortening of mice treated with normal saline (NS) or doxorubicin (Dox). Right: number of TUNEL-positive cardiomyocytes 4 weeks after doxorubicin treatment. *$P<0.05$ vs saline-treated wild type mice; #$P<0.05$ vs doxorubicin-treated wild type mice.